IEEE Open Journal of Vehicular Technology

Received 18 November 2023; accepted 24 March 2024. Date of publication 28 March 2024;
date of current version 23 April 2024. The review of this article was coordinated by Editor Sumei Sun.

Digital Object Identifier 10.1109/OJVT.2024.3382886

Full-Duplex in Massive Multiple-Input Multiple-Output

THO LE-NGOC [1] (Life Fellow, IEEE), YUANZHE GONG [1] (Graduate Student Member, IEEE), MOBEEN MAHMOOD [1] (Graduate Student Member, IEEE), ASIL KOC [1] (Graduate Student Member, IEEE), ROBERT MORAWSKI [1], JAMES GARY GRIFFITHS [2], PHILIPPE GUILLEMETTE [2], JAMAL ZAID [2] (Member, IEEE), AND PEIWEI WANG [2]

(Invited Paper)

[1]Department of Electrical and Computer Engineering, McGill University, Montreal, QC H3A 0E9, Canada
[2]Huawei Technologies Canada Company, Ltd., Ottawa, ON K2K 3J1, Canada

CORRESPONDING AUTHOR: YUANZHE GONG (e-mail: yuanzhe.gong@mail.mcgill.ca).

This work was supported in part by Huawei Technologies Canada and in part by the Natural Sciences and Engineering Research Council of Canada.

ABSTRACT In-band full-duplex (FD) operation can double the spectral efficiency of massive multiple-input multiple-output (mMIMO) systems by allowing simultaneous transmission and reception over the same time/frequency slot. However, the main challenge encountered in implementing an FD radio wireless transceiver is to greatly suppress the residual self-interference (SI) generated from its own transmitter below the receiver noise floor to avoid performance degradation in the detection of the signal of interest received from remote transmitters. It is pointed out that the single-stage digital beamforming (DBF) scheme would introduce an impractically high complexity unsuitable for implementing FD-mMIMO. This paper considers an FD hybrid beamforming (FD-HBF) scheme for multi-user (MU)-mMIMO systems, in which large SI-suppression is achieved by exploring dynamic transmitter/receiver (Tx/Rx) isolation using RF-beamforming designs, and exploiting the degrees of freedom of a large number of antenna elements in separate Tx and Rx antenna arrays, in conjunction with high-performance baseband (BB) digital fractionally-spaced (FS) SI-cancellation (SIC) techniques. This paper starts with a discussion of the main parameters and impairments (in an mMIMO transceiver) that can impact the SI-suppression performance and the proposed RF-beamforming Tx/Rx isolation and BB SI-cancellation design strategies along with their achieved performance and complexities. Joint-beamforming optimization to maximize both Tx/Rx performance and isolation is discussed with an example of a nature-inspired optimization scheme to achieve an average Tx/Rx RF isolation of 64.4 dB and the best isolation of 76 dB. The paper continues with a description of an FD-mMIMO transceiver prototype using Tx/Rx 8x8-element antenna arrays along with analytical, simulation and measured results. Illustrative results indicate that the proposed combination of RF-beamforming Tx/Rx isolation and BB digital fractionally spaced SI-cancellation can offer an overall SI suppression of more than 131 dB and bring the residual SI below the receiver noise floor.

INDEX TERMS Full-duplex, mMIMO, hybrid beamforming, antenna isolation, joint-beamforming optimization, beamforming isolation, antenna array, baseband SIC.

I. INTRODUCTION

Massive multiple-input and multiple-output (mMIMO) technology has been developed as a viable technique in response to the growing demand for high data rates and enhanced spectral efficiency in wireless communication systems [1]. This technological innovation is integral to the Fifth Generation (5G) and Beyond 5G (B5G) networks, as they exemplify a growing inclination towards employing an augmented number of antennas at the base station (BS). For instance, the third-generation partnership project (3GPP) has been

contemplating the deployment of 64-256 antenna configurations [2]. mMIMO increases the overall multi-user (MU) system capacity by leveraging a considerable number of antenna elements to form directional beams characterized by high directivity and narrow beamwidth [3], [4]. Nevertheless, the traditional half-duplex (HD) systems, i.e., time division duplexing (TDD), in which the systems alternate between transmitting and receiving, or frequency division duplexing (FDD), where systems transmit and receive in separate frequency bands, place inherent restrictions on the maximum data rate and spectrum efficiency. In contrast, when the transmitter (Tx) and receiver (Rx) operate in a full-duplex (FD) mode, the system can transmit and receive data simultaneously on the same frequency band, theoretically doubling spectral efficiency [5], [6], [7]. Integrating mMIMO with FD is anticipated to substantially augment the spectral efficiency and capacity of communication systems [8].

The impact on the receiver performance created by the possible strong self-interference (SI) from the transmitted signal of the same node can be the crucial impediment that prevents FD from being widely adopted. This is particularly critical because the received signal strength from the intended users often falls significantly below the SI power. This discrepancy is attributed to the rapid growth of path loss with distance, with receive (Rx) antennas being situated much closer to the local transmit (Tx) antennas compared to those of remote users. The excessive SI power can significantly degrade the received Signal-to-Interference-and-Noise Ratio (SINR), further constraining channel throughput [9]. To uphold FD performance under such conditions, advanced Tx/Rx isolation and self-interference cancellation (SIC) techniques are pivotal for mitigating the SI strength to near or below the noise floor [6].

A. LITERATURE REVIEW

1) ANTENNA ISOLATION

Tx/Rx isolation refers to the ability of a system to separate the transmit (Tx) and receive (Rx) signals effectively. It is achieved by preventing and minimizing the RF leakage signal between the local Tx and Rx to reduce the SI so as to operate the receiver front-end and analog-to-digital converter (ADC) in their linear range. To achieve a high RF isolation, the most direct way is antenna spacing, which increases path loss [10], [11]. In addition, the power of the captured coupling waves can be diminished by applying cross-polarization, which increases the polarization mismatch between the local Rx and Tx antennas [12], [13]. Experimental results show that RF isolation plays an essential role in FD communication, and more than 70 dB SI suppression can be achieved [10], [15].

The mMIMO technology adds more degrees of freedom that can facilitate improved spatial isolation by using narrow, steerable beams. By focusing the signal energy in a narrow scattering propagation area, it is possible to reduce the strength of the leakage wave moving in an undesirable direction. By steering and changing the interactions between the Tx and Rx beams, the beamformer design can play an essential role in the FD design. Beamforming isolation can reduce the SI intensity significantly by electronically steering the beam toward the radiation nulls of the interference source antennas [16]. Antenna and beamforming isolation design can maintain residual SI at the Rx RF chain at a sufficiently low level to avoid overloading or saturating the front-end ADC or low-noise amplifier (LNA).

2) RF BEAMFORMING ISOLATION

In recent research, the two-stage hybrid beamforming (HBF) design has gained popularity as a solution to decrease hardware complexity [17]. HBF splits the beamforming architecture into two segments: RF Tx/Rx beamforming and the digital baseband (BB) precoder/combiner. A low number of RF chains is used to connect these two segments for reduced hardware complexity and power consumption. Various HBF approaches, both for beamforming/combining in downlink/uplink directions, are examined for HD transmission in [18], [19], [20], [21], [22], [23], [24] and FD transmission in [16], [25], [26], [27], [28], [29], [30], [31]. In particular, the authors in [18] propose a joint design of RF and BB stages using full channel state information (CSI) to maximize the total sum-rate of the system. An angular-based HBF technique is proposed in [19], where the RF-stage is constructed utilizing users' angular information only. In [20], the authors propose a sub-connected HBF structure where each Tx and Rx consists of several sub-arrays and the total achievable rate is maximized using the successive interference cancellation technique. An eigen-beamforming-based HBF technique is developed using the channel covariance matrix in [21], [22], [23] for different two-dimensional array structures using both full and low-resolution hardware components. The authors then extend their work in [24] for different three-dimensional array configurations in mMIMO systems and design HBF using the channel matrix's singular value decomposition (SVD).

Regarding the FD communications in mMIMO systems, a hybrid precoding/combining (HPC) technique for millimeter-wave (mmWave) FD mMIMO systems is proposed in [31], which uses the angle-of-departure (AoD) and angle-of-arrival (AoA) information to suppress SI while also reducing the number of RF chains. The authors show that the power of the far-field (near-field) SI channel is cancelled by 81.5 dB (44.5 dB) in point-to-point FD mMIMO systems. In [25], separate and joint FD beamforming algorithms based on sequential convex programming are presented to maximize the sum-rate for both single-user (SU-) or multi-user (MU)-MIMO FD systems. In [26], a FD mmWave relaying system is considered to suppress SI while maximizing spectral efficiency using an orthogonal matching pursuit-based SI-cancellation algorithm. Similarly, a HPC design for FD amplify-and-forward (AF) mmWave relay systems is considered in [27], introducing a zero-space SIC method based on correlated mmWave channel estimation errors. A FD mmWave HBF scheme is introduced in [16] for a

MU-mMIMO system, where the non-orthogonal beams are generated to serve multiple users while suppressing the near-field component of the SI channel and maximizing the sum-rate capacity. The authors show that the proposed HBF scheme can achieve 78.1 dB of SIC in FD mMIMO systems. In [28], the authors proposed an iterative FD HBF scheme to mitigate SI by jointly designing the transmit and receive RF beamformer weights, the precoder, and combiner matrices and achieving SI suppression by up to 30 dB. The authors in [29] designed the analog and digital beamformers of a FD mMIMO system based on the practical constraints of RF chains, channel knowledge, beam alignment, and a limited receive dynamic range. A two-timescale HBF scheme for FD mmWave multiple-relay transmission is investigated in [30], where the analog and digital beams are updated based on channel samples and real-time low-dimensional effective channel state information (CSI) matrices, respectively.

By employing the instantaneous SI channel knowledge during the HBF design, the FD MU-mMIMO systems are designed to simultaneously support a single downlink UE and a single uplink UE over the same frequency band [32], and multiple downlink/uplink UEs [33], [34], where both employ the instantaneous SI channel knowledge during the HBF design are proposed. Later, a technique is developed that utilizes slow time-varying Angle of Departure (AoD) and Angle of Arrival (AoA) information at the RF stage, along with a reduced-size effective Channel State Information (CSI) at the BB stage, to improve the SIC quality in FD mMIMO [31]. Illustrative results show that hybrid techniques can approach the performance of the fully digital method with lower system complexity [17], [35], [36].

3) BASEBAND SI-CANCELLATION

The residual SI occurs when the transmitted signal leaks into the receive path of the same device or system. SIC techniques aim to suppress or cancel out this interference, allowing the device or system to effectively transmit and receive signals simultaneously. These techniques involve sophisticated algorithms and signal processing methods to estimate and subtract the SI from the received signal. The remaining SI can be further mitigated by the use of digital baseband SI-cancellation (BB-SIC) techniques, which aim to estimate the residual SI for reconstructing its counterpart and cancelling it from the received signal [6], [37]. To reconstruct the residual SI signal, the baseband (BB) sampled Tx signals before the Tx RF chains are processed by the set of adaptive FIR filters and the summed/superimposed outputs are subtracted from the corresponding Rx signals. Most commonly used structures for digital BB-SIC are based on the transversal symbol-spaced (SS) finite impulse response (FIR) filter, whose tap-delay is set to the signal's symbol interval, e.g., [38] and [39] for FD single-input single-output (SISO) and [40], [41] for FD multiple-input multiple-output (MIMO). By implementing different design algorithms, such as least-square (LS), minimum-mean-square-error (MMSE), and maximum-likelihood (ML), a set of FIR filters with tap coefficients and digitally controlled delay elements can be used to estimate the SI channel [6], [37], [40], [42]. A 16-tap BB canceller in [38] further suppressed a 400 MHz bandwidth SI by around 50 dB after an RF-SIC stage. The work in [39] implemented a BB-SIC stage directly after the antenna-level SIC to reduce the SI by around 30 dB for a low-power or short-range, single-antenna full-duplex communication system. In [41], a BB delay-based FIR filtering SI-canceller for 2×2 Full-Duplex MIMO has been implemented and up to 35/45 dB average self-interference-cancellation (SIC) across 40/20 MHz bandwidth has been achieved.

B. CONTRIBUTIONS

This paper examines an FD hybrid beamforming (FD-HBF) scheme for mMIMO (FD-HBF-mMIMO) systems, which explores large-scale Tx/Rx antenna array design and joint Tx/Rx beamforming optimization to achieve dual goals: maximizing both Tx/Rx performance and isolation by exploiting the degrees of freedom in mMIMO, in conjunction with high-performance baseband (BB) digital fractionally-spaced SIC techniques. We show that by using antenna isolation, RF beamforming, and BB-SIC in FD-HBF-mMIMO systems, we can achieve a total SI suppression of more than 131 dB, and bring the residual SI below the receiver noise floor. The main contributions are summarized as follows:

1) We consider a pair of cross-polarized 8 × 8 rectangular antenna arrays, which is designed to reduce the Tx/Rx coupling in FD-mMIMO systems. Particularly, a total of $64\times64 = 4096$ SI channels between Tx and Rx antenna are measured in an anechoic chamber with a total of 1601 sampling points between frequency range from 3 GHz to 4 GHz for each SI channel. The experimental results illustrate that an average SI isolation of 56 dB can be achieved over a bandwidth of 20 MHz (centered at 3.5 GHz) by the prototype of FD-mMIMO antenna arrays.
2) We propose the design of RF beamforming stages for both Tx and Rx to suppress the strong SI while utilizing the spatial degrees of freedom offered due to the use of large array structures. In particular, the RF beamforming stages are designed to steer the beams at uplink and downlink users with some beam perturbation within the directivity degradation constraints in Tx/Rx directions. The sample 1x4 sub-arrays demonstrate an average Tx/Rx RF isolation of 64.4 dB and the best isolation of 76 dB with the proposed RF beamforming scheme, which can avoid the need of costly RF-SIC stages.
3) We consider digital BB-SIC to jointly optimize both Tx/Rx performance as well as further suppress/cancel the residual SI (after antenna isolation and RF beamforming) by using fractionally-spaced (FS) SIC techniques. Illustrative results reveal that the FS-FIR

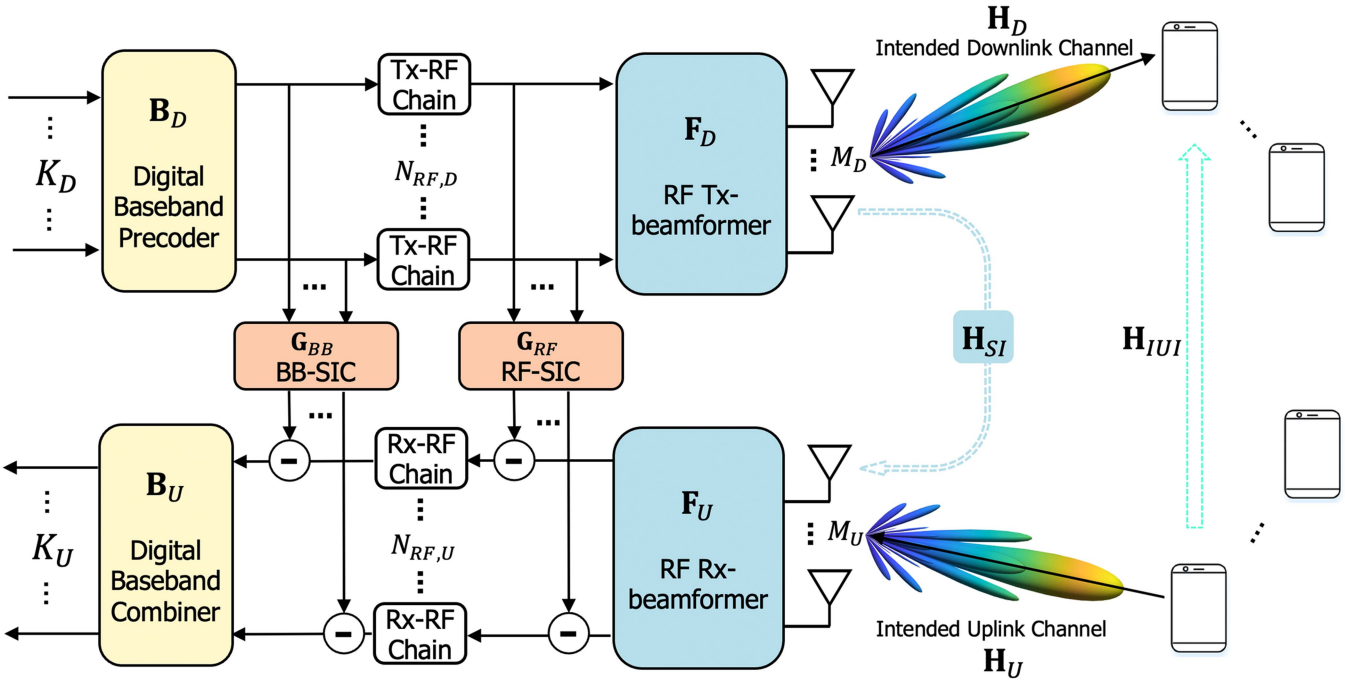

FIGURE 1. FD-HBF-mMIMO system with several SI isolation and cancellation stages.

structure can significantly improve the SIC performance with an oversampling rate larger than 1 by avoiding possible aliasing due to sampling at the symbol rate. An additional SI suppression of more than 75 dB can be achieved in the simulation via the proposed BB-SIC, which brings the residual SI to the noise floor.

C. ORGANIZATION

The rest of this paper is organized as follows. Section II introduces the proposed FD-HBF-mMIMO architecture and the system model, outlining the design methodologies employed to achieve the necessary SI isolation and cancellation. Section III delves into the design aspects of the antenna array, focusing on achieving considerable Tx/Rx isolation appropriate for FD-mMIMO and presents prototype developments and corresponding measured SI channels. Section IV examines RF Tx/Rx beamforming for FD operation, proposing an optimized joint Tx/Rx beamforming solution to minimize SI between local Tx and Rx, while maintaining directivity in both directions. The effectiveness of this proposed scheme is validated through simulation using experimentally measured SI channel data. Section V details the BB-SIC techniques utilizing a digitally fractionally-spaced FIR structure with various design criteria: LS, MMSE, and ML. Simulation results on SIC performance are presented with different oversampling rates. Section VI concludes the paper, summarizing the main findings and suggesting directions for future research.

II. FD-HBF-MMIMO ARCHITECTURE

A. SYSTEM MODEL

Fig. 1 depicts the simplified block diagram of an FD-HBF-mMIMO base-station (BS) transceiver with M_D transmit, and M_U receive antenna elements and serving K_D downlink and K_U uplink single-antenna users. We consider the downlink signal is processed through BB stage $\mathbf{B}_D \in \mathbb{C}^{N_{RF,D} \times K_D}$ and the downlink RF beamformer $\mathbf{F}_D \in \mathbb{C}^{M_D \times N_{RF,D}}$, where $N_{RF,D}$ is the number of Tx RF chains such that $K_D \leq N_{RF,D} \ll M_D$. Similarly, the received uplink signal at BS is processed through the uplink RF beamformer $\mathbf{F}_U \in \mathbb{C}^{N_{RF,U} \times M_U}$ and the uplink BB combiner $\mathbf{B}_U \in \mathbb{C}^{K_U \times N_{RF,U}}$ by utilizing $N_{RF,U}$ Rx RF chains, where $K_U \leq N_{RF,U} \ll M_U$. The uplink and downlink RF beamforming stages (i.e., $\mathbf{F}_U$ and $\mathbf{F}_D$) are built using Phase Shifters (PS), which introduce a constant-modulus (CM) constraint. Then, the received downlink $K_D \times 1$ vector signal vector can be expressed as follows:

$$\mathbf{r}_D = \underbrace{\mathbf{H}_D \mathbf{F}_D \mathbf{B}_D \mathbf{d}_D}_{\text{Desired Signal}} + \underbrace{\mathbf{w}_D}_{\text{Noise}} + \underbrace{\mathbf{H}_{IUI} \mathbf{d}_U}_{\text{IUI}}, \tag{1}$$

where the vector $\mathbf{d}_D \in \mathbb{C}^{K_D \times 1}$, $\mathbf{d}_U \in \mathbb{C}^{K_U \times 1}$, and the matrix $\mathbf{H}_D \in \mathbb{C}^{K_D \times M_D}$ represent the data signal transmitted from the BS, the data signals transmitted from the uplink users, and the downlink channel, respectively. Here, $\mathbf{w}_D \sim \mathcal{CN}(0, \sigma_w^2 \mathbf{I}_{M_D})$ is the complex circularly symmetric Gaussian noise vector, and the matrix $\mathbf{H}_{IUI} \in \mathbb{C}^{K_D \times K_U}$ is the inter-user interference (IUI) channel, which represents the interference between downlink and uplink users as they may use the same time/frequency slots.

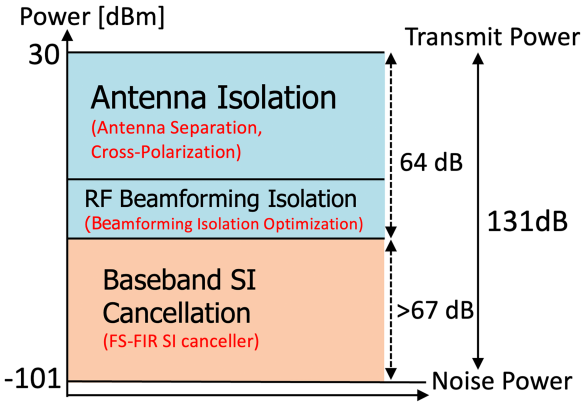

FIGURE 2. Example of performance breakdown of SI isolation and cancellation techniques (with 1x4 sub-arrays, 20 MHz bandwidth).

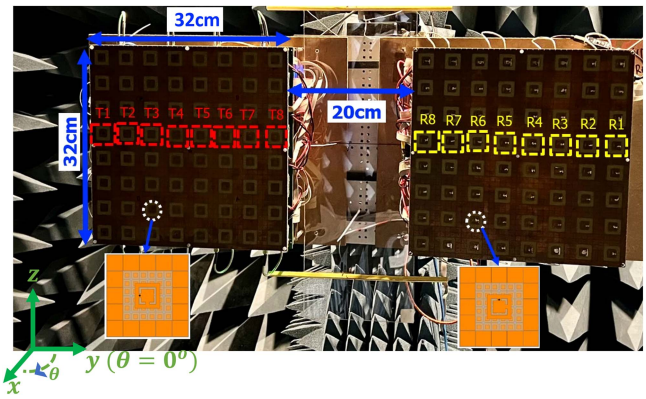

FIGURE 3. FD-mMIMO array prototype measurement in the anechoic chamber.

On the uplink, the received signal vector at the output of the uplink baseband combiner $\mathbf{B}_U$ can be represented by the $K_U \times 1$ vector as follows:

$$\mathbf{r}_U = \underbrace{\mathbf{B}_U\mathbf{F}_U\mathbf{H}_U\mathbf{d}_U}_{\text{Desired Signal}} + \underbrace{\mathbf{B}_U\mathbf{F}_U\mathbf{w}_U}_{\text{Modified Noise}} + \underbrace{\mathbf{B}_U[(\mathbf{F}_U\mathbf{H}_{SI}\mathbf{F}_D) - (\mathbf{G}_{RF} + \mathbf{G}_{BB})]\mathbf{B}_D\mathbf{d}_D}_{\text{Self-interference (SI)}}, \quad (2)$$

where the matrix $\mathbf{H}_U \in \mathbb{C}^{M_U \times K_U}$ represents the uplink channel, $\mathbf{w}_U \sim \mathcal{CN}(0, \sigma_w^2\mathbf{I}_{M_U})$ is the complex circularly symmetric Gaussian noise vector, and the matrices $\mathbf{G}_{RF}$ and $\mathbf{G}_{BB} \in \mathbb{C}^{N_{RF,U} \times N_{RF,D}}$ denote the RF-SIC and BB-SIC, respectively. The received signal at BS is the combination of the desired signal (i.e., the first term is the signal transmitted by the uplink users via channel $\mathbf{H}_U$), a modified noise (i.e., the second term is due to the Gaussian thermal noise $\mathbf{w}_U$ modified by the uplink baseband stage and RF beamformer), and the strong SI (i.e., the third term is due to the possible SI where the matrix $\mathbf{H}_{SI} \in \mathbb{C}^{M_U \times M_D}$ represents the SI channel matrix presented between Tx and Rx antennas at BS).

B. SELF-INTERFERENCE CHANNEL

The complete SI channel includes two components as [16]:

$$\mathbf{H}_{SI} = \mathbf{H}_{\text{LoS}} + \mathbf{H}_{\text{NLoS}} \in \mathbb{C}^{M_U \times M_D}, \quad (3)$$

where $\mathbf{H}_{\text{LoS}} \in \mathbb{C}^{M_U \times M_D}$ is the residual near-field SI channel via line-of-sight (LoS) paths after applying the antenna isolation, $\mathbf{H}_{\text{NLoS}} \in \mathbb{C}^{M_U \times M_D}$ is the far-field SI channel via the reflected non-line-of-sight (NLoS) paths. Due to the short distance between Tx and Rx, we can define the residual near-field SI channel via the spherical wavefront instead of the planar wavefront [31]. Then, the near-field SI channel between the $(i, j)^{th}$ transmit and $(p, q)^{th}$ receive antennas is given by (please see Fig. 3):

$$\mathbf{H}_{\text{LoS}}\left(\left[M_U^{(y)}(p-1) \;\; +q\right], \left[M_D^{(y)}(i-1)+j\right]\right) = \frac{\mu}{\Delta_{(i,j)\to(p,q)}} e^{-j2\pi\Delta(i,j)\to(p,q)}, \quad (4)$$

where $M_D^{(y)}$ and $M_U^{(y)}$ are the corresponding Tx and Rx antenna elements along y-axis, $\Delta_{(i,j)\to(p,q)}$ is the distance normalized by wavelength between the corresponding antennas, μ is the normalization scalar to satisfy $10\log_{10}(\|\mathbf{H}_{\text{LoS}}\|_F^2) = -P_{\text{ISO,dB}}$ as the residual near-field SI channel power with $P_{\text{ISO,dB}}$ as the amount of beam isolation achieved by the Tx and Rx antenna separation. The distance between $(i, j)^{th}$ Tx and $(p, q)^{th}$ Rx antenna pairs for URA configuration is calculated as [16]:

$$\Delta_{(i,j)\to(p,q)} = \Big(\big[D_x + (i-1)d + (p-1)d\cos(\Theta)\big]^2 + \big[D_y + (j-q)d\big]^2 + \big[D_z + (p-1)d\sin(\theta)\big]^2\Big)^{\frac{1}{2}}, \quad (5)$$

where $d = 0.5$ is the normalized half-wavelength distance, D_x, D_y and D_z are the distance between Tx/Rx URAs normalized by wavelength along x-axis, y axis and z-axis, respectively, and Θ is the rotation angle of receive URA along y-axis. Afterwards, the far-field SI channel $\mathbf{H}_{\text{NLOS}}$ is modeled via the planar wavefront and 3D geometry-based stochastic channel model as follows [16]:

$$\mathbf{H}_{\text{NLoS}} = \sum_{l=1}^{L_{\text{SI}}} \frac{z_{\text{SI},l}}{\tau_{\text{SI},l}^{\eta}} \mathbf{a}_U\left(\gamma_{\text{SI},U,l}^{(x)}, \gamma_{\text{SI},U,l}^{(y)}\right) \mathbf{a}_D^T\left(\gamma_{\text{SI},D,l}^{(x)}, \gamma_{\text{SI},D,l}^{(y)}\right) = \mathbf{A}_{\text{SI},U}\mathbf{Z}_{\text{SI}}\mathbf{A}_{\text{SI},D} \in \mathbb{C}^{M_U \times M_D}, \quad (6)$$

where L_{SI} is the total number of reflected NLoS paths, η is the path loss exponent, $\tau_{\text{SI},l}$ and $z_{\text{SI},l} \sim \mathcal{CN}(0, \frac{1}{L_{\text{SI}}})$ are the distance and complex path gain, respectively, $\mathbf{Z}_{\text{SI}} = \text{diag}\left(\frac{z_{\text{SI},1}}{\tau_{\text{SI},1}^{1}}, \ldots \frac{z_{\text{SL},L_{\text{SI}}}}{\tau_{\text{S},L_{\text{SI}}}}\right) \in \mathbb{C}^{L_{\text{SI}} \times L_{\text{SI}}}$ is the diagonal path gain matrix, $\mathbf{A}_{\text{SL},U} \in \mathbb{C}^{M_U \times L_{\text{SI}}}$ and $\mathbf{A}_{\text{SI},D} \in \mathbb{C}^{L_{\text{SI}} \times \bar{M}_D}$ are the Rx and Tx array phase response matrices, respectively. Here, we have $\gamma_{\text{SI},U,l}^{(x)} = \sin(\theta_{\text{SI},U,l})\cos(\psi_{\text{SI},U,l})$ and $\gamma_{\text{SI},U,l}^{(y)} = \sin(\theta_{\text{SI},U,l})\sin(\psi_{\text{SI},U,l})$ as a function of the elevation

angle-of-arrival $\theta_{\mathrm{SI},U,l} \in [\theta_{\mathrm{SI},U} - \delta^{\theta}_{\mathrm{SI},U}, \theta_{\mathrm{SI},U} + \delta^{\theta}_{\mathrm{SI},U}]$ and azimuth AoA $\psi_{\mathrm{SI},U,l} \in [\psi_{\mathrm{SI},U} - \delta^{\psi}_{\mathrm{SI},U}, \psi_{\mathrm{SI},U} + \delta^{\psi}_{\mathrm{SI},U}]$. Similarly, $\gamma^{(x)}_{\mathrm{SI},D,l}=\sin(\theta_{\mathrm{SI},D,l})\cos(\psi_{\mathrm{SI},D,l})$ and $\gamma^{(y)}_{\mathrm{SI},D,l}=\sin(\theta_{\mathrm{SI},D,l})\sin(\psi_{\mathrm{SI},D,l})$ are calculated via the elevation angle-of-departure $\theta_{\mathrm{SI},D,l} \in [\theta_{\mathrm{SI},D} - \delta^{\theta}_{\mathrm{SI},D}, \theta_{\mathrm{SI},D} + \delta^{\theta}_{\mathrm{SI},D}]$ and azimuth AoD $\psi_{\mathrm{SI},D,l} \in [\psi_{\mathrm{SI},D} - \delta^{\psi}_{\mathrm{SI},D}, \psi_{\mathrm{SI},D} + \delta^{\psi}_{\mathrm{SI},D}]$. The details of measured SI in an anechoic chamber for FD-HBF-mMIMO are presented in Section III-A.

C. MOTIVATIONS FOR SI SUPPRESSION IN FD-HBF-MMIMO

It must be noted that the third term in both (1) and (2) does not exist in traditional HD operation since the downlink transmission and uplink reception are in different time/frequency slots. As a result, the detection performance of the HD system is mainly limited by the thermal Gaussian noise term and can be determined by the operating signal-to-noise ratio (SNR).

In comparison, the downlink users in FD communications can experience two sources of interference: 1) multi-user interference due to the different downlink users; and 2) inter-user interference due to uplink users (i.e., $\mathbf{H}_{IUI}\mathbf{d}_U$). Similarly, in the case of uplink transmission, the inter-user interference from multiple uplink users as well as the strong SI at BS are the main sources of interference. By using effective precoding/beamforming solutions, possible multi-user interference due to multiple users on the same link (i.e., uplink or downlink) can be mitigated by BS via the joint design of the digital BB combiner ($\mathbf{B}_U$) and analog RF Rx-beamformer ($\mathbf{F}_U$) on the uplink and/or the joint design of the digital BB precoder ($\mathbf{B}_D$) and analog RF Tx-beamformer ($\mathbf{F}_D$) on the downlink [16], [43]. Moreover, the presence of the third term of non-zero inband (or co-channel) SI impacts the detection performance of FD communications systems. For FD operation with similar detection performance as HD, it is required to keep this SI term as small as possible, ideally below the thermal Gaussian noise term. For example, consider a transmission using a signal bandwidth of 20 MHz with the signal $\mathbf{d}_D$ transmitted power of 30 dBm. The thermal Gaussian noise power in over 20 MHz bandwidth is -174 dBm/Hz+$10\log_{10}(20\ \mathrm{MHz}) = -101$ dBm, implying that the SI term must be kept lower than -101 dBm, or 131 dB lower than the transmitted power. This required significant SI suppression is the critical challenge in designing FD communications systems. Investigating the third term, it can be seen that this SI term can be suppressed by making $[(\mathbf{F}_U\mathbf{H}_{SI}\mathbf{F}_D) - (\mathbf{G}_{RF} + \mathbf{G}_{BB})] \approx 0$. This can be achieved by different solutions, which are as follows:

1) proper antenna design with additional consideration to reduce the Tx/Rx coupling represented by $\mathbf{H}_{SI}$,
2) proper RF Tx and Rx beamformer design with additional consideration to make $\mathbf{F}_U\mathbf{H}_{SI}\mathbf{F}_D \approx 0$.

Conceptually, the above approaches aim to isolate the Tx and Rx sides. Hence, we call them SI-isolation approaches. If such isolation approaches are not sufficient to suppress the SI, additional SI cancellation can be done at RF with $\mathbf{G}_{RF}$ RF-SIC or/and at baseband with $\mathbf{G}_{BB}$ BB-SIC to suppress the SI further. By SI cancellation (SIC), we consider designing the $N_{RF,U} \times N_{RF,D}$ matrices $\mathbf{G}_{RF}$ and $\mathbf{G}_{BB}$ to estimate the residual effective SI channel ($\mathbf{F}_U\mathbf{H}_{SI}\mathbf{F}_D$) seen by the SIC stages, i.e., $\mathbf{G}_{RF} + \mathbf{G}_{BB} \approx \mathbf{F}_U\mathbf{H}_{SI}\mathbf{F}_D$, and remove it from the Rx signal, i.e., $[(\mathbf{F}_U\mathbf{H}_{SI}\mathbf{F}_D) - (\mathbf{G}_{RF} + \mathbf{G}_{BB})] \approx 0$.

From the above discussions, the RF-SIC and BB-SIC have a similar function, and $\mathbf{G}_{RF}$ and $\mathbf{G}_{BB}$ have the same size of $N_{RF,U} \times N_{RF,D}$. Their design considers estimating the response of ($\mathbf{F}_U\mathbf{H}_{SI}\mathbf{F}_D$) in the time or frequency domain. Normally, time-domain approaches using transversal filters to adaptively estimate the impulse response of ($\mathbf{F}_U\mathbf{H}_{SI}\mathbf{F}_D$) are preferred for their relatively simple structure.

As RF-SIC operates at RF, the adaptive tapped-delay-line (TDL) transversal filters have to be implemented in the RF analog domain, which are complicated with limited tap length. Alternatively, RF-SIC can use adaptive finite-impulse-response (FIR) filters in the digital baseband domain and then up-converted to the RF analog domain by using separate auxiliary Tx RF chains. While this alternative RF-SIC design can make use of simple digital FIR filters, the required separate auxiliary Tx RF chains represent additional complexity, hardware costs, size, and power consumption.

On the other hand, BB-SIC operates at baseband, using simple adaptive digital FIR filters, and hence, is preferred over RF-SIC. However, since the Rx-RF chains include an LNA and front-end analog-to-digital converters (ADC) with limited effective dynamic range, the residual SI at the input of the Rx-RF chains must be kept sufficiently low to prevent the LNA/ADC from saturating and overloading, which will cause non-linear signal distortion. In other words, if the designed RF Tx and Rx beamformers can make $\mathbf{F}_U\mathbf{H}_{SI}\mathbf{F}_D$ sufficiently small so that the residual SI does not overload the Rx-RF chains, then only BB-SIC can be used for simplicity. Otherwise, RF-SIC is needed to keep the Rx-RF chains operating in the normal linear region without increasing the noise floor.

If FD-mMIMO is implemented using the single-stage digital beamforming (DBF), there is only the baseband precoder $\mathbf{B}_D$ and combiner $\mathbf{B}_U$, i.e., $\mathbf{F}_U, \mathbf{F}_D = \mathbf{I}$ (identity matrix) and the sizes of $\mathbf{B}_D$ and $\mathbf{B}_U$ are $M_D \times K_D$ and $K_U \times M_U$, respectively, with $M_D \gg N_{RF,D}$ transmit and $M_U \gg N_{RF,U}$ receive RF chains. As a result, the third (SI) term becomes $\mathbf{B}_U[\mathbf{H}_{SI} - (\mathbf{G}_{RF} + \mathbf{G}_{BB})]\mathbf{B}_D\mathbf{d}_D$. Then, we can deduce the following:

1) RF Tx/Rx beamforming for SI-isolation is not available,
2) impractically large-size $M_U \times M_D$ RF-SIC is needed to keep the M_U Rx-RF chains operating in the normal linear regions,
3) impractically large-size $M_U \times M_D$ BB-SIC.

In other words, single-stage digital beamforming (DBF) is not suitable for FD-mMIMO. On the other hand, hybrid beamforming (HBF) is not only a suitable approach but also facilitates the FD-mMIMO. The massive number of antenna elements in mMIMO that are intended to make narrow beams to serve multi-user (MU) operation effectively, can be further explored to design the Tx and Rx beams for efficient SI-isolation jointly. The efficient and effective SI isolation,

in turn, ensures the SI level low enough to maintain a linear operation of the Rx RF chains without the need for RF-SIC, simplifying the FD SIC implementation.

An example of the achievable SI isolation and cancellation in the FD design of this work is highlighted in Fig. 2. We employ Tx-to-Rx antenna separation and cross-polarization to mitigate Tx-to-Rx antenna mutual coupling (MC). Subsequently, a perturbation-based beamforming isolation optimization approach, constrained by beam directivity degradation, is utilized to suppress beam level MC even further, yielding an average total isolation of 64.4 dB. Following these stages, a baseband precoding approach is implemented to minimize residual SI, subsequently achieving a SIC in excess of 67 dB. The integration of these multifarious techniques enables the attainment of over 131 dB in SI attenuation, effectively equating the SI to the noise level.

III. ANTENNA ISOLATION DESIGN FOR FD-MMIMO

A. ANTENNA ARRAY DESIGN STRUCTURE

As an example, we consider an 8x8Tx-to-8x8Rx rectangular antenna array structure designed for FD-mMIMO, which operates in the 3.35–3.6 GHz frequency band, shown in Fig. 3. The structure incorporates two cross-polarized 8×8 arrays that are spaced 20 cm apart. Each of these two arrays consists of 64 dual-layer electromagnetic bandgap (EBG) slotted circularly polarized patch antenna elements [44], [45]. Notably, the slots' directions on the central radiation patches for both the Tx and Rx elements are mirrored. This design choice ensures the attainment of an orthogonal circular polarization by the Tx and Rx antennas. Furthermore, in the array, each neighbouring element has a center-to-center separation distance of 4.00 cm, equivalent to $0.47\lambda_0$ (λ_0 is the free-space wavelength and equals to 8.6 cm at 3.5 GHz), to prevent grating lobes during beamforming. Consequently, the dimensions of each 8x8 antenna array are $W_T = 32$ cm in width and $L_T = 32$ cm in length.

B. SI CHANNEL MEASUREMENT SETUP

The measurement of the SI channel between the Tx and Rx elements is conducted within an anechoic chamber with dimensions 6.1 m $\times$ 2.4 m $\times$ 2.4 m ($length \times width \times height$) and equipped with C-RAM SFC-48 RF absorber to minimize reflections and external interference. A vector network analyzer (VNA) with an output power of 10 dBm is used. To minimize the number of connections, the VNA connects to Tx and Rx antennas through RF switches. Then, the resulting parameters are collected by a PC via an Ethernet cable. A total of $64 \times 64 = 4096$ SI channels between the 64 Tx elements to the 64 Rx elements are measured. For each Tx-to-Rx antenna element pair, the S-parameter data is collected for a total of 1601 sampling points between frequency range from 3 GHz to 4 GHz (i.e., a bandwidth of 1 GHz with a sample step size of 0.625 MHz). The parameters in the form of. S2P file are collected and combined to get the SI channel matrix 64x64 SI channel matrix $\mathbf{H}_{SI,ALL} \in \mathbb{C}^{64\times64\times1601}$.

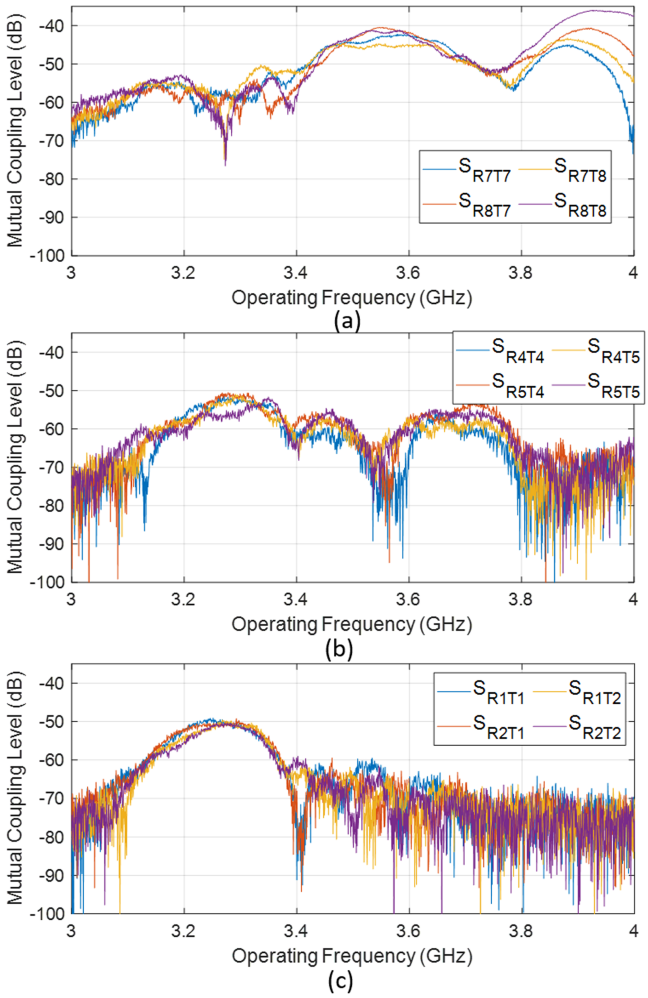

FIGURE 4. Measured S-parameter magnitude plots of sample Tx-to-Rx antenna element pairs: (a) closest: T7/T8 to R7/R8; (b) elements at the array centers: T4/T5 to R4/R5; (c) farthest: T1/T2 to R1/R2.

C. MEASURED SI CHANNEL

Across the 4096 SI channels, we achieve a consistent average mutual coupling (MC) level of -53.2 dB,[1] at 3.5 GHz. Within the frequency bands of 20 MHz (3.49 to 3.51 GHz) and 100 MHz (3.45 to 3.55 GHz), an average MC value level of -56.0 dB and -55.9 dB can be achieved, respectively.

Considering the extensive number of Tx-to-Rx element pairs, we present the magnitude plot of measured S-parameters (in dB) for three representative pairs (closest: T7/T8 to R7/R8; elements at the array centers: T4/T5 to R4/R5; farthest: T1/T2 to R1/R2) in Fig. 4. As the distance between the Tx and Rx antennas grows, along with the increase in the number of EBG elements placed between them, a

[1]This study utilizes geometric means to characterize the average mutual coupling (MC) or isolation level, as the mutual coupling value represents a ratio of the received power (Rx) to the transmitted power (Tx). For averaging MC power across a bandwidth, where it signifies the cumulative power within the operating frequencies, an arithmetic mean is employed to depict the average MC within a band.

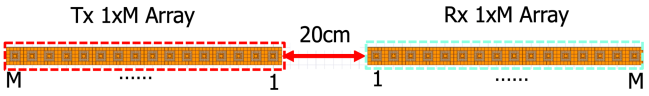

FIGURE 5. Simulation setup for array length versus beam mutual coupling.

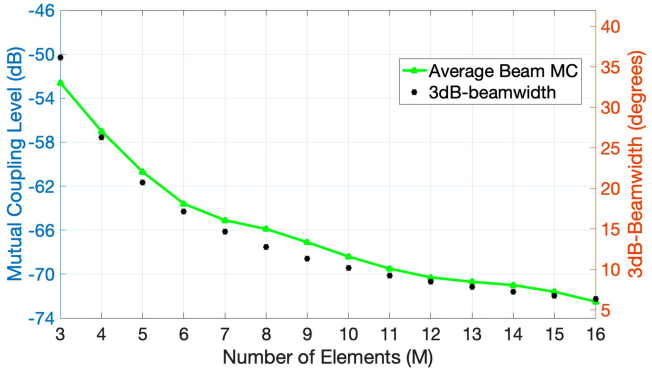

FIGURE 6. 3 dB-beamwidth and average beam mutual coupling versus the number of elements (M) in two Tx/Rx orthogonally-polarized 1×M ULAs (simulation results).

substantial enhancement in Tx-to-Rx isolation is observed. At 3.5 GHz, the mutual coupling (MC) values have been found to average at −44.2 dB, −60.8 dB, and −65.7 dB in Fig. 4(a), (b), and (c), respectively. Furthermore, when the analysis is extended over bandwidths of 20 MHz and 100 MHz, the variation of average MC values within the bandwidth is less than 1.7 dB, compared with the values at center frequency 3.5 GHz.

D. TX/RX ARRAY BEAM ISOLATION

Antenna arrays play a crucial role in enhancing spatial isolation by employing two principal mechanisms: 1) the generation of highly directional beams that focus radiation power towards the intended user, substantially minimizing power leakage into potential interference paths; 2) focus the radiation power towards the directions where interference is nullified, reducing the receiver's sensitivity to interference power detection.

The MC between the Tx and Rx sub-arrays, as a function of beam steering angles, can be estimated by the weighted sum of the contributions of element-wise MC, i.e., for a pair of 1×M uniform linear Tx and Rx sub-arrays, the MC expression can be given as

$$S_b(M, \theta_D, \theta_U) = \sum_{j=1}^{M}\sum_{i=1}^{M} w_i^*(\theta_D) w_j^*(\theta_U) S_{ji}, \qquad (7)$$

where S_{ji} is the complex S-parameter that represents the coupling between the Tx antenna element i and the Rx antenna element j in the sub-array. $w_i(\theta_D)$ and $w_j(\theta_U)$ are the complex steering weights for the Tx element i and Rx element j at the downlink beamforming angle θ_D and uplink beamforming angle θ_U in the azimuth plane.

1) BEAMWIDTH AND ISOLATION (SIMULATION)

Given the constraints inherent in hardware, executing experimental measurements on a length-adjustable linear array poses substantial challenges. To circumvent these difficulties, we first opt to utilize Ansys HFSS simulation, a highly realistic simulation platform, in this section to elucidate the relationship between beamwidth and beam MC levels when Tx-Rx array separation is kept at the same separation distance. Fig. 5 illustrates the simulation setup, featuring two Tx/Rx orthogonally-polarized $1 \times M$ Uniform Linear Arrays (ULA) based on the proposed antenna element structure. The two arrays are positioned with an edge-to-edge separation distance of 20 cm (the same separation as our antenna array prototype).

The simulation results on mutual coupling (MC) S_{ji} between Tx element i and Rx element j at 3.5 GHz are used to estimate the beam MC between the Tx and Rx $1 \times M$ arrays at various steering angles based on (7). The Tx/Rx array length M varies from 3 to 16 and beam steering angle ranges $\{\theta_D, \theta_U\} \in [45^\circ : 0.1^\circ : 135^\circ]$.

The relationship between the average beam MC and 3 dB-beamwidth in comparison to the number of elements (M) is depicted in Fig. 6. It is evident that with the increment in M from 3 to 16, there is a discernible improvement in average beam-level isolation, characterized by a reduction in the average beam MC by 19.9 dB. Specifically, the average beam MC decreases from −52.6 dB to −72.5 dB, in tandem with the contraction of the 3 dB-beamwidth from 36 degrees to 6 degrees. The converging decline of both the beam MC and 3 dB-beamwidth unveils a prominent correlation, suggesting that a decrement in beamwidth is coupled with an enhancement in beam-level isolation, as the array length increases. The MC improvement and 3 dB-beamwidth reduction tend to shrink as M > 10. Further increasing M to 16 results in a reduction in average beam MC of less than 5 dB.

Beam MC versus Tx/Rx steering angles with six sample Tx/Rx array lengths and $\{\theta_D, \theta_U\} \in [0^\circ$ to $180^\circ]$ are presented in Fig. 7. It can be observed larger and more dense Tx-to-Rx isolation angle pairs (with MC≤-70 dB) can be observed. For a $1 \times M$ array, a $M - 1$ radiation null will be created in the beamforming process and lead to a decrease in the neighbouring radiation null distance. The reduction in the distance between high-isolation Tx/Rx beam angle pairs, which results in a higher fraction of high-isolation (θ_D, θ_U) pairs in the steering range, is the primary factor contributing to the improvement in average isolation.

2) BEAMWIDTH AND ISOLATION (MEASURED RESULTS)

The measured SI channel information presented in Section III.B is used as the S_{ji} at 3.5 GHz in (7) to estimate and investigate the beam MC variation versus the sub-array lengths. The Tx/Rx sub-arrays located at the fourth row of the arrays shown in Fig. 3 with a separation of 20 cm are steering within a range $\{\theta_D, \theta_U\} \in [45^\circ : 0.1^\circ : 135^\circ]$. The Tx/Rx $1 \times M$ sub-arrays comprise elements from T/R 8 to T/R $(9 - M)$, as

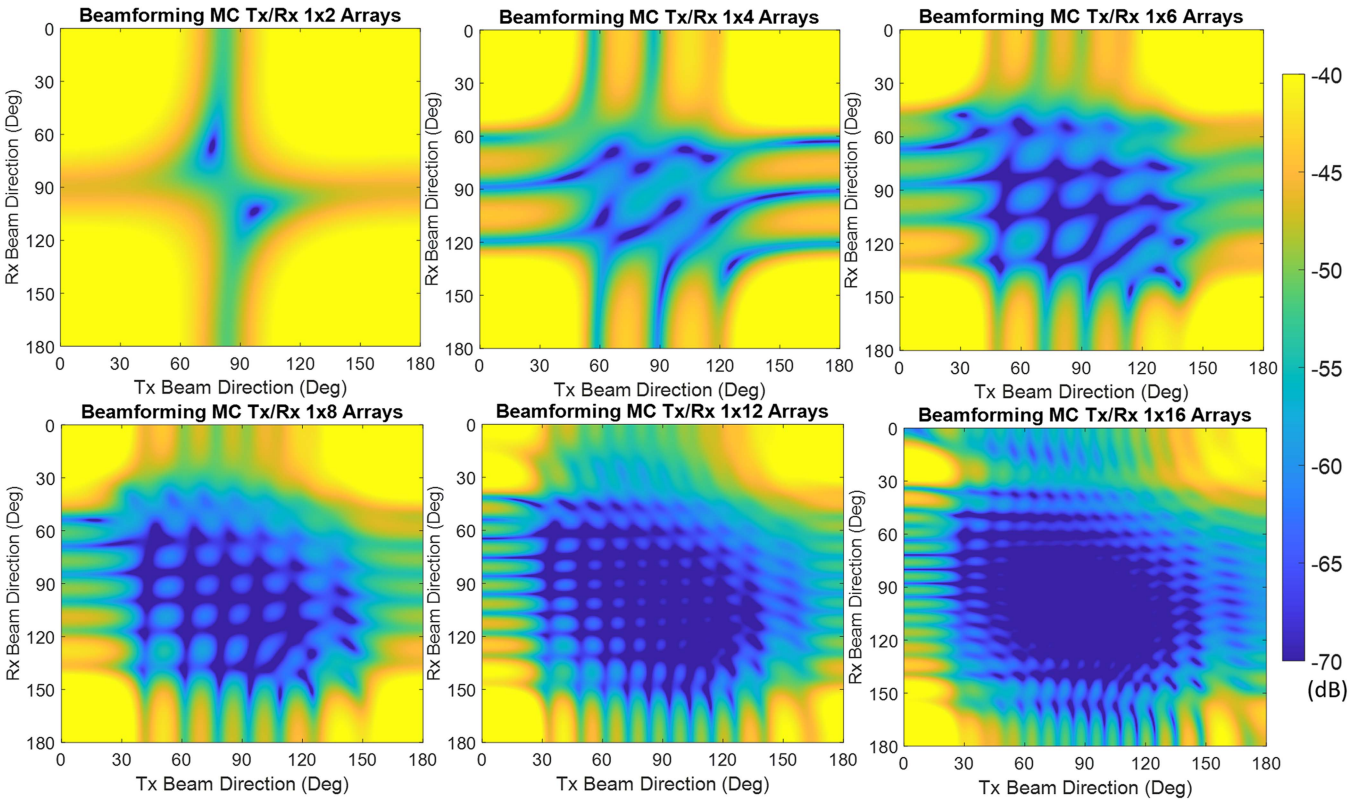

FIGURE 7. Simulation results of Tx/Rx beam mutual coupling within steering range 0° to 180° of 1x2, 1x4, 1x6, 1x8, 1x12, and 1x16 arrays at 3.5 GHz.

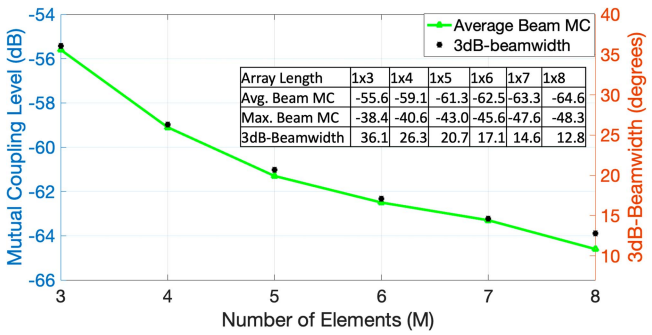

Array Length	1x3	1x4	1x5	1x6	1x7	1x8
Avg. Beam MC	-55.6	-59.1	-61.3	-62.5	-63.3	-64.6
Max. Beam MC	-38.4	-40.6	-43.0	-45.6	-47.6	-48.3
3dB-Beamwidth	36.1	26.3	20.7	17.1	14.6	12.8

FIGURE 8. 3 dB-beamwidth and average beam mutual coupling versus number of elements (M) in 1×M ULAs (measured results).

labeled in Fig. 3. The achieved average MC level and the sub-array beamwidth (when θ=0°) versus number of elements (M) in $1 \times M$ ULAs (measured results) are presented in Fig. 8. The changes of the average beam MC (in dB) follow a similar trend compared with the sub-array beamwidth. Both the average and maximum MC values demonstrate that by confining radiation power in a limited scattering area, spatial isolation can be significantly improved. As the sub-array length increases from 1×3 to 1×8, the average beam MC decreases by 9 dB, and the maximum (worst case) beam MC decreases by 9.9 dB. The results based on the measured SI channel are consistent with the results from the HFSS simulations.

IV. RF BEAMFORMING FOR ENHANCED ISOLATION IN FD-MMIMO

The ability of the antenna arrays to produce directional, narrow beams concentrates the radiated power in the intended direction and reduces power leakage toward the nearby Rx. In FD operation, the beamforming optimization design aims to further lower SI between the local Tx and Rx while maintaining the power intensity towards the target direction. The large number of antenna elements in mMIMO can provide increased degrees of freedom to effectively serve the joint optimization with multiple objectives, i.e., joint Tx/Rx RF beamforming, $\mathbf{F}_U$ and $\mathbf{F}_D$, to maximize both Tx/Rx performance (in terms of Tx/Rx sum-rate or capacity or directivity) and Tx/Rx isolation (by suppressing $\mathbf{F}_U\mathbf{H}_{SI}\mathbf{F}_D \approx 0$) [52]. This general approach can be formulated for various interesting optimization problems to solve. Based on the Tx and Rx RF beamforming stages, the total achieved SI mitigation between Tx and Rx is given as:

$$A_{\mathrm{SI}} = 10\log_{10}\left(\frac{1}{N}\sum\nolimits_n \left|\mathbf{F}_U^T(\hat{\theta}_U)\mathbf{H}_{SI}(:,:,n)\mathbf{F}_D(\hat{\theta}_D)\right|^2\right), \quad (8)$$

where $n = 1, 2, \ldots, N$ is the sample frequency point for a total of N frequency points in a given bandwidth. Let $\mathbf{\Phi}_D(\theta_D)$ and $\mathbf{\Phi}_U(\theta_U)$ be the phase response vectors in the Tx and Rx directions,

$$\mathbf{\Phi}_D(\theta_D) = [1, e^{-j2\pi d\cos(\theta_D)}, \cdots, e^{-j2\pi d(M_D-1)\cos(\theta_D)}]^T \in \mathbb{C}^{M_D\times 1}, \tag{9}$$

$$\mathbf{\Phi}_U(\theta_U) = [1, e^{j2\pi d\cos(\theta_U)}, \cdots, e^{j2\pi d(M_U-1)\cos(\theta_U)}]^T \in \mathbb{C}^{M_U\times 1}. \tag{10}$$

Let $\hat{\theta}_D$ and $\hat{\theta}_U$ be the beam steering azimuth angles of the Tx and Rx beams, respectively. Then, the Tx and Rx RF beamformers can be written as

$$\mathbf{F}_D(\hat{\theta}_D) = \frac{1}{\sqrt{M_D}}[1, e^{j2\pi d\cos(\hat{\theta}_D)}, \cdots, e^{j2\pi d(M_D-1)\cos(\hat{\theta}_D)}]^T \in \mathbb{C}^{M_D\times 1}, \tag{11}$$

$$\mathbf{F}_U(\hat{\theta}_U) = \frac{1}{\sqrt{M_U}}[1, e^{-j2\pi d\cos(\hat{\theta}_U)}, \cdots, e^{-j2\pi d(M_U-1)\cos(\hat{\theta}_U)}]^T \in \mathbb{C}^{M_U\times 1}. \tag{12}$$

If we steer the Tx and Rx beams to the desirable directions (i.e., $\hat{\theta}_U = \theta_U$, $\hat{\theta}_D = \theta_D$), then the Tx and Rx directivities reach their maxima as:

$$|\mathbf{\Phi}_D^T(\theta_D)\mathbf{F}_D(\theta_D)|^2 = M_D, \quad |\mathbf{F}_U^T(\theta_U)\mathbf{\Phi}_U(\theta_U)|^2 = M_U. \tag{13}$$

For an FD-mMIMO system consisting of Tx and Rx RF beamformers $\mathbf{F}_D$ and $\mathbf{F}_U$, the total achieved SI suppression can be maximized by the joint optimization of Tx and Rx beam steering angles $\hat{\theta}_D$, $\hat{\theta}_U$. We can formulate the optimization problem for achieved SI as follows:

$$\begin{aligned} \max_{\{\hat{\theta}_D,\hat{\theta}_U\}} \quad & \frac{1}{N}\sum\nolimits_n \left|\mathbf{F}_U^T(\hat{\theta}_U)\mathbf{H}_{SI}(:,:,n)\mathbf{F}_D(\hat{\theta}_D)\right|^2 \\ \text{s.t.} \quad & C_1: \ M_D - |\mathbf{\Phi}_D^T(\theta_D)\mathbf{F}_D(\hat{\theta}_D)|^2 \le \epsilon, \\ & C_2: \ M_U - |\mathbf{F}_U^T(\hat{\theta}_U)\mathbf{\Phi}_U(\theta_U)|^2 \le \epsilon, \end{aligned} \tag{14}$$

where C_1 and C_2 refer to the directivity degradation constraints in DL and UL directions, respectively. In other words, the constraints mean that we limit the degradation of directivities from the main beam (desirable) directions θ_D and θ_U to a small value ϵ. The optimization problem defined in (9) is non-convex and intractable due to the non-linearity constraints. The interference level can be mitigated by directing the beams toward the radiation nulls of the unwanted sources of interference. In this proposed Min-SI-BF scheme, our objective is to suppress the strong SI for an FD-mMIMO system. Particularly, we introduce beam perturbations to design the RF beamforming stages for the following reasons: 1) the maximum number of beams that can be steered at the exact user location is limited by the number of Tx and Rx antennas;[2] 2) the maximum-directivity beamforming (i.e., steering the Tx and Rx beams at exact user locations) can only minimize strong SI at certain Tx-Rx (θ_D, θ_U) angle-pairs. Compared to the RF beamforming scheme based on phase-range constraint in [16], this proposed min-SI-BF scheme under directivity-loss constraint allows more freedom to perturb the Tx and Rx beams. Moreover, the min-SI-BF scheme under phase-range constraint in [16] is limited by the quantized users' AoD and AoA pairs, where the Tx and Rx beams are steered within the boundary of the quantized angles. Thus, for a small number of antennas, the quantization process can introduce large errors, which can result in reduced directivity gain. On the other hand, the quantization error can be low for a large number of antennas, however, the perturbed beams can only be steered within tight boundaries, so the beamforming-based SI mitigation might be limited. Instead of using quantized angle pairs in this work, we allow the Tx and Rx beams to be slightly steering away from the AoD and AoA angles to minimize the SI power while maintaining possible degradation in directivity within affordable constraints. In particular, the proposed min-SI-BF approach optimizes the Tx and Rx RF beamformers via new perturbed angles for enhanced SI suppression in FD-mMIMO systems. For a given angle-pair $\{\theta_D, \theta_U\}$, we introduce a beam-perturbation to create a new angle-pair (i.e., $\{\hat{\theta}_D, \hat{\theta}_U\}$) to suppress SI.

We propose a particle swarm optimization (PSO)-based perturbation scheme to solve the challenging non-convex optimization problem (14). The algorithm starts with a swarm of N_p particles, each with its own position, velocity, and fitness value, which are randomly placed in the optimization search space of perturbation coefficients. During a total of T iterations, the particle p communicates with others, and moves for the exploration of the optimization space to find the optimal solution. We define the perturbation vector $\mathbf{X}_p^{(t)}$ as:

$$\mathbf{X}_p^{(t)} = [\hat{\theta}_D^p, \hat{\theta}_U^p], \tag{15}$$

where $p = 1, \ldots, N_p$ and $t = 0, 1, \ldots, T$. For each p^{th} particle, by substituting (15) in (11) and (12), the Tx and Rx RF beamformers $\mathbf{F}_D(\mathbf{X}_p^{(t)})$ and $\mathbf{F}_U(\mathbf{X}_p^{(t)})$ can be obtained as function of perturbation angles $\hat{\theta}_D^p$ and $\hat{\theta}_U^p$, respectively. By using (8), we can write the achieved SI mitigation as:

$$A_{\text{SI}}(\mathbf{X}_p^{(t)}) = 10\log_{10}\left(\frac{1}{N}\sum_n \left|\mathbf{F}_U^T(\mathbf{X}_p^{(t)})\mathbf{H}_{SI}(\mathbf{X}_p^{(t)})\mathbf{F}_D(\mathbf{X}_p^{(t)})\right|^2\right). \tag{16}$$

[2]The number of Tx/Rx beam pairs for maximum directivity is bounded by the size of the antenna array. Thus, it can become a bottleneck in scenarios with a large number of users or high user density. As the number of Tx and Rx users increases, the available Tx-Rx angle pairs for maximum directivity with minimum SI may be exhausted, leading to reduced system capacity and throughput.

Algorithm 1: Proposed Min-SI-BF RF Stages Design Algorithm.

Input: $N_p, T, M_D, M_U, \mathbf{H}_{SI}, (\theta_D.\theta_U)$.
Output: $\hat{\theta}_D, \hat{\theta}_U$.
for $t = 0 : T$ **do**
  for $n = 1 : N_p$ **do**
    if t = *0* **then**
      Initialize the velocity as $\mathbf{v}_p^{(0)} = \mathbf{0}$.
      Initialize $\mathbf{X}_p^{(t)}$ uniformly distributed in $[\mathbf{X}_{\text{Low}}, \mathbf{X}_{\text{Upp}}]$.
    else
      Update the velocity $\mathbf{v}_p^{(t)}$ via (19).
      Update the perturbation $\mathbf{X}_p^{(t)}$ via (20).
    end
    Find the personal best $\mathbf{X}_{p,\text{best},n}^{(t)}$ via (17).
  end
  Find the global best $\mathbf{X}_{\text{best}}^{(t)}$ as in (18).
  Design RF stages $\mathbf{F}_D$, $\mathbf{F}_U$ via (21),(22).
end

At the t^{th} iteration, the personal best for the p^{th} particle and the current global best among all particles are respectively found as:

$$\mathbf{X}_{\text{best},p}^{(t)} = \arg\max_{\mathbf{X}_p^{(t^*)}, \forall t^*=0,1,\ldots,t} A_{\text{SI}}(\mathbf{X}_p^{(t^*)}), \tag{17}$$

$$\mathbf{X}_{\text{best}}^{(t)} = \arg\max_{\mathbf{X}_{\text{best},p}^{(t)}, \forall p=0,1,\ldots,N_p} A_{\text{SI}}(\mathbf{X}_{\text{best},p}^{(t)}). \tag{18}$$

The convergence of the proposed PSO-based perturbation scheme for enhanced SI suppression depends on the velocity vector $\mathbf{v}_p$ for both personal best $\mathbf{X}_{\text{best},p}$ and global best $\mathbf{X}_{\text{best}}$ solutions, which is defined as:

$$\mathbf{v}_p^{(t+1)} = \mathbf{\Omega}_1(\mathbf{X}_{\text{best}}^{(t)} - \mathbf{X}_p^{(t)}) + \mathbf{\Omega}_2(\mathbf{X}_{\text{best},p}^{(t)} - \mathbf{X}_p^{(t)}) + \mathbf{\Omega}_3^{(t)} v_p^{(t)}, \tag{19}$$

where $\mathbf{v}_p^{(t)}$ is the velocity of the p^{th} particle at the t^{th} iteration, $\mathbf{\Omega}_1, \mathbf{\Omega}_2$ are the random diagonal matrices with the uniformly distributed entries over [0,2] and represent the social relations among the particles, and the tendency of a given particle for moving towards its personal best, respectively. Here, $\mathbf{\Omega}_3 = (\frac{T-1}{T})\mathbf{I}_{(2N_D+2N_U)}$ is the diagonal inertia weight matrix, which finds the balance between exploration and exploitation for optimal solution in search space. By using (19), the position of each particle during t^{th} iteration is updated as:

$$\mathbf{X}_p^{(t+1)} = \text{clip}\left(\mathbf{X}_p^{(t)} + \mathbf{v}_p^{(t+1)}, \mathbf{X}_{\text{Low}}, \mathbf{X}_{\text{Upp}}\right), \tag{20}$$

where $\mathbf{X}_{\text{Low}} \in \mathbb{R}^{(2N_D+2N_U)}$ and $\mathbf{X}_{\text{Upp}} \in \mathbb{R}^{(2N_D+2N_U)}$ are the lower-bound and upper-bound vectors for the perturbation coefficients, respectively, and are constructed according to the earlier defined boundaries of each perturbation coefficient given in C_1 and C_2. Here, we define $\text{clip}(x, a, b) = \min(\max(x, a), b)$ as the clipping function to avoid exceeding the bounds. Furthermore, different from the sub-optimal approach, we here consider each perturbation coefficient as a continuous variable inside its boundary. Then, we can design the perturbation-based RF beamforming stages as:

$$\mathbf{F}_D(\hat{\theta}_D) = \frac{1}{\sqrt{M_D}}[1, e^{j2\pi d\cos(\hat{\theta}_D)}, \cdots, e^{j2\pi d(M_D-1)\cos(\hat{\theta}_D)}]^T, \tag{21}$$

$$\mathbf{F}_U(\hat{\theta}_U) = \frac{1}{\sqrt{M_U}}[1, e^{-j2\pi d\cos(\hat{\theta}_U)}, \cdots, e^{-j2\pi d(M_U-1)\cos(\hat{\theta}_U)}]^T. \tag{22}$$

The proposed perturbation-based RF stages design for SI minimization using PSO is summarized in Algorithm 1. Fig. 9 compares the achieved SI suppression for the proposed beam perturbation-based RF beamforming scheme with maximum directivity scheme using 4 antenna elements (i.e., 1×4 array for both Tx and Rx). We consider the downlink and uplink UE to be located at angular locations $\theta_D = 105^\circ$ and $\theta_U = 45^\circ$, respectively. Based on the maximum directivity scheme, as shown in Fig. 9(a), the beams are directed in the desired UE directions θ_D, θ_U, and we can achieve a SI suppression of -50.3 dB. However, based on the proposed RF beamforming scheme, beam perturbations are introduced in both uplink and downlink directions. As a result, the RF stages direct the beams at $\hat{\theta}_D$ and $\hat{\theta}_U$ (i.e., $\mathbf{F}_D(\hat{\theta}_D)$ and $\mathbf{F}_U(\hat{\theta}_U)$). The proposed beamforming scheme then finds the optimal perturbations as 95° and 58° for downlink and uplink beams, respectively, and achieves a SI suppression of around -58.2 dB at the expense of directivity degradation of $\epsilon = 2$ dB. In essence, introducing perturbations in both the downlink and uplink directions

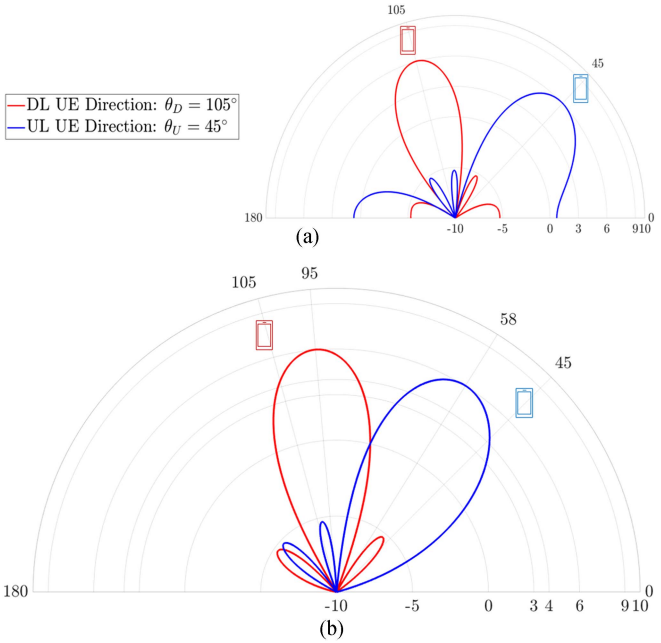

FIGURE 9. RF Beamforming using 1×4 sub-array. (a) Maximum directivity. (b) Proposed beam perturbation.

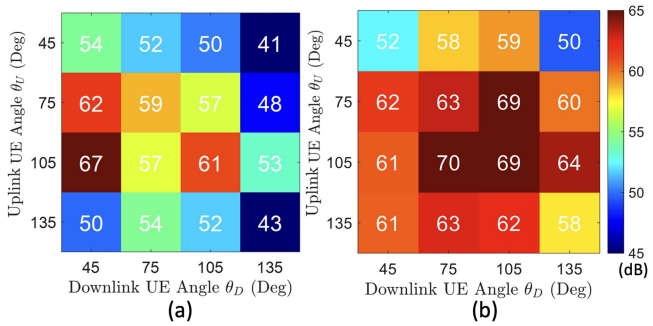

FIGURE 10. Beam Isolation using (a) 1x4 sub-arrays and (b) 1x8 sub-arrays over 20 MHz bandwidth.

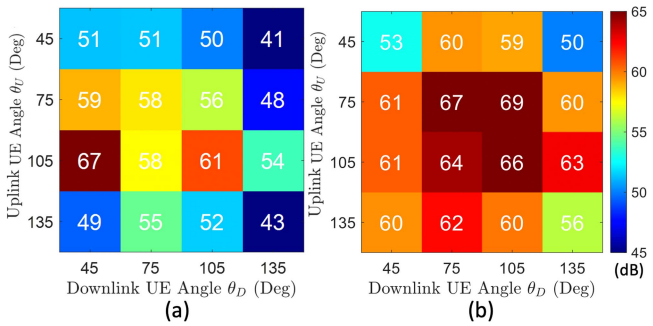

FIGURE 11. Beam Isolation using (a) 1x4 sub-arrays and (b) 1x8 sub-arrays over 100 MHz bandwidth.

yields an additional SI suppression gain of 7.9 dB, that the residual SI power is 6 times smaller compared to the SI level without the beamforming optimization.

A. SIMULATION SETUP BASED ON MEASURED SI CHANNEL

As detailed in Section III-B, the measured SI channel matrix, $\mathbf{H}_{SI,ALL}$, provides a realistic and comprehensive dataset for assessing beam-level isolation optimization strategies. In the simulation, we consider ULA sub-array configurations of 4 and 8 antenna elements for both Tx and Rx. In line with the 3GPP specifications, which state that the uplink (UL) and downlink (DL) channel bandwidth (BW) may range from 5 MHz to 100 MHz [46], therefore, in our simulation two operating bandwidths, which are 20 MHz (i.e., 3.49 GHz to 3.51 GHz) or 100 MHz (i.e., 3.45 GHz to 3.55 GHz), are considered.

B. BEAM-LEVEL ISOLATION WITHOUT OPTIMIZATION

Fig. 10 presents the isolation level without the proposed isolation optimization scheme for sample 1×4 and 1×8 sub-arrays over 20 MHz bandwidth. We consider four different angular locations for both uplink and downlink UE (i.e., $\{\theta_D, \theta_U\} \in [45^\circ : 30^\circ : 135^\circ]$).

It can be seen by steering the beams at the exact user location with 1×4 sub-array can provide an average beam isolation of 53.7 dB with a maximum isolation of around 67 dB (at $\theta_D = 45^\circ, \theta_U = 105^\circ$). Meanwhile, using a larger sub-array, for instance, 1×8, can increase the average beam isolation to 61.2 dB with maximum isolation of 70 dB (i.e., $\theta_D = 75^\circ, \theta_U = 105^\circ$). The results indicate an average isolation improvement of 7.5 dB in the 20 MHz bandwidth when 1x8 sub-arrays are used, compared with the average isolation using 1x4 sub-arrays.

The same trend can be seen in Fig. 11 for 100 MHz bandwidth, where a 1×4 sub-array can provide beam isolation ranging from 41 dB to 67 dB with an average isolation of 53.3 dB. Similarly, a 1×8 sub-array can provide an average beam isolation of 60.6 dB with a maximum isolation of 67 dB, which indicates an isolation improvement of 7.3 dB compared with the average Tx-to-Rx 1x4 sub-array isolation across a 100 MHz bandwidth. The larger number of frequency points in 100 MHz bandwidth results in less than 0.6 dB degradation in beam isolation when compared to the results with bandwidth of 20 MHz.

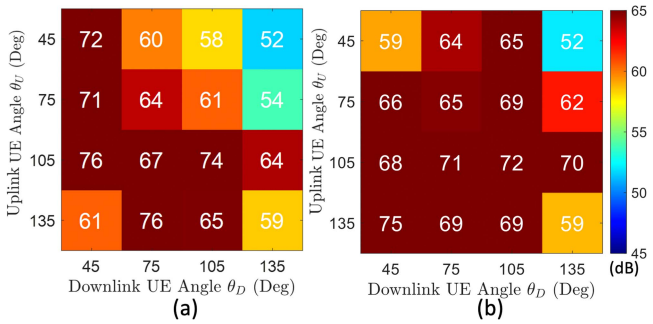

FIGURE 12. Beam Isolation with perturbation-based optimization using (a) 1x4 sub-arrays and (b) 1x8 sub-arrays over 20 MHz bandwidth.

C. BEAM-LEVEL ISOLATION WITH PERTURBATION-BASED OPTIMIZATION

Fig. 12 presents the achieved beam isolation for 1×4 and 1×8 sub-arrays over 20 MHz bandwidth using the proposed beam-perturbation-based RF beamforming scheme. We consider four different angular locations for both uplink and downlink UE (i.e., $\{\theta_D, \theta_U\} \in [45^\circ : 30^\circ : 135^\circ]$). It can be seen that by introducing beam perturbations in both uplink and downlink directions at the expense of directivity degradation of $\epsilon = 2$ dB, we can achieve an average beam isolation of around 64.4 dB with maximum isolation of 76 dB (i.e., $\theta_D = 75^\circ, \theta_U = 135^\circ$). This represents an average isolation gain of around 10.7 dB when compared to the case of maximum directivity (i.e. when beams are steered at exact user locations as shown in Fig. 10. Except for four (θ_D, θ_U) pairs, all the other test cases achieve a beam isolation better than 60 dB. In contrast, without the proposed isolation optimization mechanism, 13 (θ_D, θ_U) pairs have an isolation worse than 60 dB.

By using a larger sub-array, 1×8 can increase the average beam isolation to around 66.0 dB with maximum isolation of

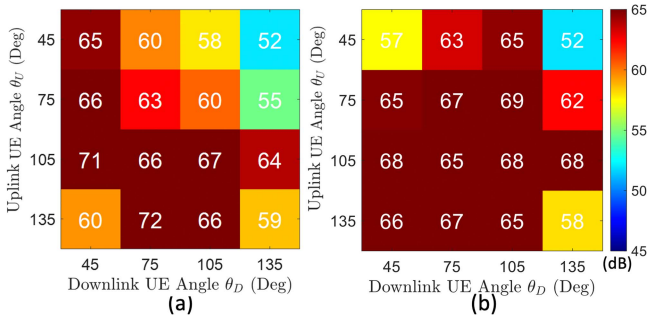

FIGURE 13. Beam Isolation with perturbation-based optimization using (a) 1x4 sub-arrays and (b) 1x8 sub-arrays over 100 MHz bandwidth.

75 dB (i.e., $\theta_D = 45°, \theta_U = 135°$). Except for three (θ_D, θ_U) pairs, all the other test cases achieve a beam isolation better than 62 dB. It is also evident that, when the perturbation-based beam isolation optimization is implemented, the average beam MC difference between the 1×8 and 1×4 sub-arrays is reduced.

Similarly, Fig. 13 shows the achieved beam isolation for 100 MHz bandwidth, where a 1×4 sub-array can provide beam isolation ranging from 52 dB to 72 dB with an average isolation of around 62.6 dB. On the other hand, a 1×8 sub-array can provide an average beam isolation of around 64.1 dB with a maximum isolation of 69 dB. As the operating bandwidth expands from 20 MHz to 100 MHz, the effectiveness of the high-isolation Tx/Rx beam pairs, which have an isolation better than 70 dB, degrades, resulting in an average isolation degradation of approximately 1.9 dB. The results show that the design of RF beamforming stages using the proposed beam-perturbation scheme can significantly enhance beam isolation.

V. DIGITAL BB-SIC

After applying Tx/Rx beamforming to jointly maximize both Tx/Rx performance and Tx/Rx isolation, the effective SI-channel is $\mathcal{H}_{\rm SI} = \mathbf{F}_U \mathbf{H}_{SI} \mathbf{F}_D$ with dimension $N_{RF,U} \times N_{RF,D}$. As discussed, further SI suppression can be performed by RF-SIC or BB-SIC or both. By using HBF, the dimension is significantly reduced to $N_{RF,U} \times N_{RF,D}$, as compared to the case using DBF with $M_U \times M_D$. In other words, mMIMO is reduced to MIMO via HBF and the RF-SIC or BB-SIC for FD-mMIMO at this point is similar to the case of FD-MIMO. On the other hand, HBF for mMIMO facilitates the Tx/Rx beamforming to jointly maximize both Tx/Rx performance and Tx/Rx isolation to provide much weaker SI sufficient to keep the Rx-RF chain (ADC/LNA) operating in a normal manner without being overloaded. After the antenna and beamforming isolation, the residual SI power will be mitigated to the dynamic range of the Rx-RF chain (ADC/LNA). RF-SIC can be omitted for simplicity and digital BB-SIC is considered for further SI suppression.

On the other hand, propagation channel impulse response can be sampled at a sampling rate faster than the symbol rate to avoid potential aliasing and hence to enhance the channel estimation [47]. In the following, we propose a fractionally spaced (FS) transversal FIR structure, where the delay element is $1/N$ of the symbol interval, for a more accurate estimation of the SI channel and hence better BB digital SIC in FD-mMIMO wireless communication systems.

The impulse response of the effective $N_{RF,U} \times N_{RF,D}$ SI-channel $\mathcal{H}_{\rm SI} = \mathbf{F}_U \mathbf{H}_{SI} \mathbf{F}_D$ can be modelled by an L-tap FS-FIR structure as $\mathbf{H}^{\rm si} = [\mathcal{H}_{\rm SI}(0), \mathcal{H}_{\rm SI}(1), \ldots, \mathcal{H}_{\rm SI}(L-1)]$ with dimension $(N_{RF,U} \times N_{RF,D}L)$. Correspondingly, we estimate it by an $(N_{RF,U} \times N_{RF,D}L)$ matrix $\mathbf{H}_{\rm e} = [\mathbf{G}_{BB}(0), \mathbf{G}_{BB}(1), \ldots, \mathbf{G}_{BB}(L-1)]$ using an L-tap FS-FIR structure whose $(N_{RF,U} \times N_{RF,D}L)$ tap-coefficients need to be derived with the general goal to make $\mathbf{H}_{\rm e} \approx \mathbf{H}^{\rm si}$ so that $\mathcal{H}_{\rm SI} - \mathbf{G}_{BB} \approx 0$. The BB-SIC performance can depend on the algorithm used to optimize the FIR coefficients. For example, the simulation results in [48] indicated that Maximum-Likelihood (ML) based SI-channel estimation outperforms the Least-Square (LS) counterpart. In the following, we develop three algorithms: LS, Minimum-Mean-Square-Error (MMSE), and ML, to estimate the SI channel and derive the $(N_{RF,U} \times N_{RF,D}L)$ tap-coefficients.

Consider the case in the absence of the intended signals from uplink users. The received uplink signal contains only the SI and noise:

$$\mathbf{r}_U = \underbrace{\mathbf{B}_U[(\mathbf{F}_U \mathbf{H}_{SI} \mathbf{F}_D) - (\mathbf{G}_{RF} + \mathbf{G}_{BB})]\mathbf{B}_D \mathbf{d}_D}_{\text{Self-interference (SI)}} + \underbrace{\mathbf{B}_U \mathbf{F}_U \mathbf{w}_U}_{\text{Modified Noise}} . \tag{23}$$

In this case, the estimation of the SI channel is affected by noise. Let $\mathbf{X}_t$ be the known Tx signal matrix formed from the known $\mathbf{B}_D \mathbf{d}_D$ and $\mathbf{Y}_t$ be the corresponding Rx signal matrix observed at the input of the digital baseband combiner in Fig. 1. For an estimated $\mathbf{H}_e$, the squared error $\mathbf{S}$ between the received signal $\mathbf{Y}_t$ and its estimated $\mathbf{X}_t \mathbf{H}_e$ is

$$\mathbf{S} = (\mathbf{Y_t} - \mathbf{X_t H_e})^{\mathbf{H}} (\mathbf{Y_t} - \mathbf{X_t H_e}) . \tag{24}$$

Using the least-square (LS) criterion, the estimated FIR coefficients $\mathbf{H}_{e,LS}$ is found when the vector gradient of $\mathbf{S}$ with respect to $\mathbf{H}_e$ is zero [49]:

$$\mathbf{H}_{e,LS} = \left(\mathbf{X}_t{}^H \mathbf{X}_t\right)^{-1} \mathbf{X}_t{}^H \mathbf{Y}_t . \tag{25}$$

The MMSE takes the expectation of $\mathbf{S}$ over all samples in $\mathbf{Y}_t$ and sets the vector gradient of the expectation with respect to $\mathbf{H}_e$ to zero. As a result, the MMSE solution is [50]:

$$\mathbf{H}_{e,MMSE} = \left(\mathbb{E}\left[\mathbf{X}_t^H \mathbf{X}_t\right]\right)^{-1} \mathbb{E}\left[\mathbf{X}_t^H \mathbf{Y}_t\right] . \tag{26}$$

In the presence of the intended signals from uplink users, ML can be used. It exploits the knowledge of both the known transmitted signals from the transmitter of the same transceiver and the known pilot symbols from the remote

transmitter to estimate the SI and the intended signals jointly. In the presence of the intended signals, we consider $\mathbf{H} = [\mathbf{H}^{si}, \mathbf{H}^{p}]$ as the extended channel coefficient matrix to be estimated and $\mathbf{D}_t = [\mathbf{X}_t, \mathbf{S}_t^p]$ as the matrix gathering both the known transmitted signals and known pilots. Including T blocks in the estimation procedure, the log-likelihood function of $\mathbf{H}$ is:

$$\mathcal{L}(\mathbf{H}) = -T \log |\mathbf{R}| - \sum_{t=1}^{T} (\mathbf{Y}_t - \mathbf{D}_t\mathbf{H})^H \mathbf{R}^{-1} (\mathbf{Y}_t - \mathbf{D}_t\mathbf{H}). \tag{27}$$

By maximizing $\mathcal{L}$ in (27), we obtain the ML estimation of $\mathbf{H}$. To solve the problem in a low-complexity manner, we consider an iterative procedure [6]. If $\mathbf{H}$ is known, $\mathcal{L}$ can be maximized by the covariance matrix $\mathbf{R}$:

$$\mathbf{R}_{ML}(\mathbf{H}) = \frac{1}{T} \sum_{t=1}^{T} (\mathbf{Y}_t - \mathbf{D}_t\mathbf{H}) (\mathbf{Y}_t - \mathbf{D}_t\mathbf{H})^H. \tag{28}$$

Inversely, if $\mathbf{R}$ is given, the solution of $\mathbf{H}$ that maximizes $\mathcal{L}(\mathbf{H})$ is:

$$\mathbf{H}_{ML}(\mathbf{R}) = \left(\sum_{t=1}^{T} \mathbf{D}_t^H \mathbf{R}^{-1} \mathbf{D}_t \right)^{-1} \sum_{t=1}^{T} \mathbf{D}_t^H \mathbf{R}^{-1} \mathbf{Y}_t. \tag{29}$$

The ML criterion iterates between (28) and (29). At iteration i, $\mathbf{H}_i$ is calculated by $\mathbf{H}_i = \mathbf{H}_{ML}(\mathbf{R}_{i-1})$ where $\mathbf{R}_{i-1}$ is the estimated covariance matrix obtained at iteration $i-1$. Afterward, $\mathbf{R}_i$ is updated by $\mathbf{R}_i = \mathbf{R}_{ML}(\mathbf{H}_i)$. The algorithm is initialized with $\mathbf{R}_0 = \mathbf{I}_{MM}$ where $\mathbf{I}_{MM}$ is an $M \times M$ identity matrix. As proven in [40], by each iteration, the log-likelihood function is increased after each iteration:

$$\mathcal{L}(\mathbf{H}_i, \mathbf{R}_i) \geq \mathcal{L}(\mathbf{H}_i, \mathbf{R}_{i-1}) \geq \mathcal{L}(\mathbf{H}_{i-1}, \mathbf{R}_{i-1}). \tag{30}$$

The iteration stops when there is no significant difference between two consecutive estimates [6].

The proposed digital BB-SIC approaches are simulated and evaluated with the FD-mMIMO transceiver prototype. OFDM transmission over a bandwidth of 20 MHz is considered. The FFT size of the OFDM signals is 64. The power amplifier (PA) is assumed to operate in a linear region with an output of +30 dBm, and the LNA/ADC at the receiver is assumed to have a sufficiently wide dynamic range to avoid overloading, with ideal non-distorted Tx signals.[3] The system thermal noise is modelled as AWGN with a power spectral density of −174 dBm/Hz, which is −101 dBm integrated over the 20 MHz signal bandwidth. In the simulation, a Tx-to-Rx antenna isolation of 56 dB is assumed. This value corresponds to the average Tx-to-Rx antenna element isolation within a 20 MHz bandwidth (3.49 GHz to 3.51 GHz) as presented in Section III-C and is also close to the worst isolation encountered during beamforming optimization as shown in Fig. 12(a). As it is possible to sample the channel impulse response at a rate higher than the symbol rate, this can help to reduce the chance of aliasing and improve channel estimation and modelling since the SI channel is not discrete nor limited to the bandwidth of the signal. To properly evaluate the design, the performance of the fractionally spaced BB digital SIC with N = 4 is also simulated.

[3]The practical impairments, like non-linear Tx amplifiers, and the receiver's effective ADC dynamic range, will limit practically achievable BB-SIC and total SIC.

TABLE 1. BB-SIC Performance With AWGN = −101 Dbm for LS, MMSE, and ML

	Tx-Rx Antenna Isolation (dB)	56		
	BB-SIC Algorithm	LS	MMSE	ML
N=1	BB-SIC (dB)	42	45	47
	Total SIC (dB)	98	101	103
N=4	BB-SIC (dB)	75	75	75
	Total SIC (dB)	131	131	131

TABLE 2. BB-SIC Performance Without AWGN for LS, MMSE, and ML

	Tx-Rx Antenna Isolation (dB)	56		
	BB-SIC Algorithm	LS	MMSE	ML
N=1	BB-SIC (dB)	42	45	47
	Total SIC (dB)	98	101	103
N=4	BB-SIC (dB)	100	104	108
	Total SIC (dB)	156	160	164

The simulation results of the digital BB-SIC are summarized in Table 1, and details of the results can be found in [51]. For N = 1 (i.e., delay element of 1 symbol interval), BB-SIC achieves 42 dB, 45 dB, and 47 dB, with LS, MMSE, ML algorithms. Increasing N = 4 improves the BB-SIC performance to 75 dB for all three algorithms. It can be observed that the BB-SIC performance of 48 dB corresponding to a total SI reduction of 131 dB is limited by the AWGN floor of −101 dBm so the total power of residual SI and AWGN is also −101 dBm.

To assess the complete capabilities and performance of the proposed BB-SIC techniques, simulations were carried out without the restriction of a noise floor limitation. The results from these simulations are summarized in Table 2. When applying an oversampling rate of N = 4 in the simulation, all three algorithms demonstrated impressive SI cancellation levels ranging from 100 dB to 108 dB. The findings emphatically highlight the efficacy of the proposed BB-SIC technique, demonstrating its capability to reduce the residual Self-Interference (SI) power to levels at or below the noise floor, thereby ensuring the robust performance of FD communications.

VI. CONCLUSION

We have considered a full-duplex hybrid beamforming (FD-HBF) architecture suitable for MU-mMIMO systems. For FD operation with the same detection performance as its HD counterpart, the SI must be kept sufficiently lower than the receiver noise floor. As a result, the required large SI suppression is a key challenge in designing FD MU-mMIMO transceivers, which can be obtained by proper SI isolation and cancellation strategies. By exploiting the available degrees of freedom of mMIMO, joint Tx/Rx RF beamforming designs can maximize both the Tx/Rx beamforming gains towards the target Tx/Rx directions and the Tx/Rx isolation to attain the low SI levels at the inputs of the Rx RF-chains required to avoid overloading the front-end LNA/ADC. Subsequently, only one baseband digital FS-FIR SI canceller can be used to offer an overall SI suppression sufficiently large to bring the residual SI below the receiver noise floor. Illustrative results indicate that a complicated and power-hungry RF-SIC stage can be eliminated for cost and power reduction. Furthermore, joint Tx/Rx RF beamforming designs can be formulated as various multi-objective, non-convex optimization problems, which nature-inspired and/or machine-learning-based techniques can solve. As a continuation, we will consider developing machine-learning-based joint Tx/Rx RF beamforming design techniques to replace the PSO-based algorithm for faster operation and further efficient machine-learning-based joint Tx/Rx RF beamforming and BB-SIC schemes.

REFERENCES

[1] S. A. Busari, K. M. S. Huq, S. Mumtaz, L. Dai, and J. Rodriguez, "Millimeter-wave massive MIMO communication for future wireless systems: A survey," *IEEE Commun. Surveys Tuts.*, vol. 20, no. 2, pp. 836–869, Secondquartter, 2018.

[2] 3GPP, "5G; Study on scenarios and requirements for next generation access technologies," 3GPP, Sophia Antipolis, France, Tech. Rep. 38.913, May 17, 2022. [Online]. Available: https://cdn.standards.iteh.ai/samples/65613/34a39b71d5fc43cabf517b474a3bcfe0/ETSI-TR-138-913-V17-0-0-2022-05-.pdf

[3] P. Xingdong, H. Wei, Y. Tianyang, and L. Linsheng, "Design and implementation of an active multibeam antenna system with 64 RF channels and 256 antenna elements for massive MIMO application in 5G wireless communications," *IEEE China Commun.*, vol. 11, no. 11, pp. 16–23, Nov. 2014.

[4] S. Malkowsky et al., "The world's first real-time testbed for massive MIMO: Design, implementation, and validation," *IEEE Access*, vol. 5, pp. 9073–9088, 2017.

[5] A. Sabharwal, P. Schniter, D. Guo, D. W. Bliss, S. Rangarajan, and R. Wichman, "In-band full-duplex wireless: Challenges and opportunities," *IEEE J. Sel. Areas Commun.*, vol. 32, no. 9, pp. 1637–1652, Sep. 2014.

[6] T. Le-Ngoc and A. Masmoudi, *Full-Duplex Wireless Communications*. Cham, Switzerland: Springer, 2017.

[7] Z. Zhang, K. Long, A. V. Vasilakos, and L. Hanzo, "Full-duplex wireless communications: Challenges, solutions, and future research directions," *Proc. IEEE*, vol. 104, no. 7, pp. 1369–1409, Jul. 2016.

[8] G. C. Alexandropoulos, M. A. Islam, and B. Smida, "Full-duplex massive multiple-input, multiple-output architectures: Recent advances, applications, and future directions," *IEEE Veh. Technol. Mag.*, vol. 17, no. 4, pp. 83–91, Dec. 2022.

[9] F. Chen, H. H. Lee, R. Morawski, and T. Le-Ngoc, "RF/Analog self-interference canceller for 2×2 MIMO full-duplex transceiver," in *Proc. IEEE Int. Conf. Commun.*, 2017, pp. 1–6.

[10] E. Everett, A. Sahai, and A. Sabharwal, "Passive self-interference suppression for full-duplex infrastructure nodes," *IEEE Trans. Wireless Commun.*, vol. 13, no. 2, pp. 680–694, Feb. 2014.

[11] M. Duarte et al., "Design and characterization of a full-duplex multi-antenna system for WiFi networks," *IEEE Trans. Veh. Technol.*, vol. 63, no. 3, pp. 1160–1177, Mar. 2014.

[12] B. Debaillie et al., "Analog/RF solutions enabling compact full-duplex radios," *IEEE J. Sel. Areas Commun.*, vol. 32, no. 9, pp. 1662–1673, Sep. 2014.

[13] H. Nawaz and I. Tekin, "Dual-polarized, differential fed microstrip patch antennas with very high interport isolation for full-duplex communication," *IEEE Trans. Antennas Propag.*, vol. 65, no. 12, pp. 7355–7360, Dec. 2017.

[14] J. Zhang, J. Li, and J. Chen, "Mutual coupling reduction of a circularly polarized four-element antenna array using metamaterial absorber for unmanned vehicles," *IEEE Access*, vol. 7, pp. 57469–57475, 2019.

[15] D. Korpi, M. Heino, C. Icheln, K. Haneda, and M. Valkama, "Compact inband full-duplex relays with beyond 100 dB self-interference suppression: Enabling techniques and field measurements," *IEEE Trans. Antennas Propag.*, vol. 65, no. 2, pp. 960–965, Feb. 2017.

[16] A. Koc and T. Le-Ngoc, "Intelligent non-orthogonal beamforming with large self-interference cancellation capability for full-duplex multiuser massive MIMO systems," *IEEE Access*, vol. 10, pp. 51771–51791, May 2022.

[17] M. Rihan, T. A. Soliman, C. Xu, L. Huang, and M. I. Dessouky, "Taxonomy and performance evaluation of hybrid beamforming for 5G and beyond systems," *IEEE Access*, vol. 8, pp. 74605–74626, 2020.

[18] X. Wu, D. Liu, and F. Yin, "Hybrid beamforming for multi-user massive MIMO systems," *IEEE Trans. Commun.*, vol. 66, no. 9, pp. 3879–3891, Sep. 2018.

[19] A. Koc, A. Masmoodi, and T. Le-Ngoc, "3D Angular-based hybrid precoding and user grouping for uniform rectangular arrays in massive MU-MIMO systems," *IEEE Access*, vol. 8, pp. 84689–84712, 2020.

[20] D. Zhang, Y. Wang, X. Li, and W. Xiang, "Hybridly connected structure for hybrid beamforming in mmWave massive MIMO systems," *IEEE Trans. Commun.*, vol. 66, no. 2, pp. 662–674, Feb. 2018.

[21] M. Mahmood, A. Koc, and T. Le-Ngoc, "Energy-efficient MU-massive-MIMO hybrid precoder design: Low-resolution phase shifters and digital-to-analog converters for 2D antenna array structures," *IEEE Open J. Commun. Soc.*, vol. 2, pp. 1842–1861, 2021.

[22] M. Mahmood, A. Koc, and T. Le-Ngoc, "2D antenna array structures for hybrid massive MIMO precoding," in *Proc. IEEE Glob. Commun. Conf.*, 2020, pp 1–6.

[23] M. Mahmood, A. Koc, and T. Le-Ngoc, "Massive-MIMO hybrid precoder design using few-Bit DACs for 2D antenna array structures," in *Proc. IEEE Int. Conf. Commun.*, 2021, pp 1–5.

[24] M. Mahmood, A. Koc, and T. Le-Ngoc, "3-D antenna array structures for millimeter wave multi-user massive MIMO hybrid precoder design: A performance comparison," *IEEE Commun. Lett.*, vol. 26, no. 6, pp. 1393–1397, Jun. 2022.

[25] S. Huberman and T. Le-Ngoc, "MIMO full-duplex precoding: A joint beamforming and self-interference cancellation structure," *IEEE Trans. Wireless Commun.*, vol. 14, no. 4, pp. 2205–2217, Apr. 2015.

[26] Y. Zhang, M. Xiao, S. Han, M. Skoglund, and W. Meng, "On precoding and energy efficiency of full-duplex millimeter-wave relays," *IEEE Trans. Wireless Commun.*, vol. 18, no. 3, pp. 1943–1956, Mar. 2019.

[27] Z. Luo, L. Zhao, H. Liu, and R. Zhang, "Robust hybrid precoding/combining designs for full-duplex millimeter wave relay systems," *IEEE Trans. Veh. Technol.*, vol. 70, no. 9, pp. 9577–9582, Sep. 2021.

[28] K. Satyanarayana, M. El-Hajjar, P. Kuo, A. Mourad, and L. Hanzo, "Hybrid beamforming design for full-duplex millimeter wave communication," *IEEE Trans. Veh. Technol.*, vol. 68, no. 2, pp. 1394–1404, Feb. 2019.

[29] I. P. Roberts, J. G. Andrews, and S. Vishwanath, "Hybrid beamforming for millimeter wave full-duplex under limited receive dynamic range," *IEEE Trans. Wireless Commun.*, vol. 20, no. 12, pp. 7758–7772, Dec. 2021.

[30] Y. Cai, K. Xu, A. Liu, M. Zhao, B. Champagne, and L. Hanzo, "Two-timescale hybrid analog-digital beamforming for mmWave full-duplex MIMO multiple-relay aided systems," *IEEE J. Sel. Areas Commun.*, vol. 38, no. 9, pp. 2086–2103, Sep. 2020.

[31] A. Koc and T. Le-Ngoc, "Full-duplex mmWave massive MIMO systems: A joint hybrid precoding/combining and self-interference cancellation design," *IEEE Open J. Commun. Soc.*, vol. 2, pp. 754–774, 2021.
[32] J. M. B. da Silva, A. Sabharwal, G. Fodor, and C. Fischione, "1-bit phase shifters for large-antenna full-duplex mmWave communications," *IEEE Trans. Wireless Commun.*, vol. 19, no. 10, pp. 6916–6931, Oct. 2020.
[33] K. Satyanarayana, M. El-Hajjar, A. A. M. Mourad, and L. Hanzo, "Multiuser full duplex transceiver design for mmWave systems using learning aided channel prediction," *IEEE Access*, vol. 7, pp. 66068–66083, 2019.
[34] M. Darabi, A. C. Cirik, and L. Lampe, "Transceiver design in millimeter wave full-duplex multi-user massive MIMO communication systems," *IEEE Access*, vol. 9, pp. 165394–165408, 2021.
[35] T. Le-Ngoc and R. Mai, *Hybrid Massive MIMO Precoding in Cloud-RAN*. Cham, Switzerland: Springer, 2019.
[36] A. F. Molisch et al., "Hybrid beamforming for massive MIMO: A survey," *IEEE Commun. Mag.*, vol. 55, no. 9, pp. 134–141, Sep. 2017.
[37] K. E. Kolodziej, B. T. Perry, and J. S. Herd, "In-band full-duplex technology: Techniques and systems survey," *IEEE Trans. Microw. Theory Techn.*, vol. 67, no. 7, pp. 3025–3041, Jul. 2019.
[38] H. Luo, M. Holm, and T. Ratnarajah, "Design and analysis of wideband self-interference cancellation for full-duplex wireless networks," in *Proc. IEEE Wireless Commun. Netw. Conf.*, 2022, pp. 2697–2702.
[39] M. S. Amjad, H. Nawaz, K. Ozsoy, O. Gurbuz, and I. Tekin, "A low-complexity full-duplex radio implementation with a single antenna," *IEEE Trans. Veh. Technol.*, vol. 67, no. 3, pp. 2206–2218, Mar. 2018.
[40] M. B. Dastjerdi, S. Jain, N. Reiskarimian, A. Natarajan, and H. Krishnaswamy, "Analysis and design of a full-duplex two-element MIMO circulator-receiver with high TX power handling exploiting MIMO RF and shared-delay baseband self-interference cancellation," *IEEE J. Solid-State Circuits*, vol. 54, no. 12, pp. 3525–3540, Dec. 2019.
[41] M. B. Dastjerdi, S. Jain, N. Reiskarimian, A. Natarajan, and H. Krishnaswamy, "28.6 full-duplex 2×2 MIMO circulator-receiver with high TX power handling exploiting MIMO RF and shared-delay baseband self-interference cancellation," in *Proc. IEEE Int. Solid- State Circuits Conf.*, 2019, pp. 448–450.
[42] Z. Gao, L. Dai, D. Mi, Z. Wang, M. A. Imran, and M. Z. Shakir, "MmWave massive-MIMO-based wireless backhaul for the 5G ultra-dense network," *IEEE Wireless Commun.*, vol. 22, no. 5, pp. 13–21, Oct. 2015.
[43] N. Fatema, G. Hua, Y. Xiang, D. Peng, and I. Natgunanathan, "Massive MIMO linear precoding: A survey," *IEEE Syst. J.*, vol. 12, no. 4, pp. 3920–3931, Dec. 2018.
[44] Y. Gong, R. Morawski, H. H. Lee, and T. Le-Ngoc, "A miniaturized 8x8 dual-layer EBG slotted circularly polarized patch antenna array for mMIMO," in *Proc. IEEE Glob. Commun. Conf.*, 2022, pp. 6511–6516.
[45] S. Ghosh, T.-N. Tran, and T. Le-Ngoc, "Dual-layer EBG-based miniaturized multi-element antenna for MIMO systems," *IEEE Trans. Antennas Propag.*, vol. 62, no. 8, pp. 3985–3997, Aug. 2014.
[46] 3GPP, "5G; NR; Base station (BS) radio transmission and reception," 3GPP, Sophia Antipolis, France, Tech. Specification 38.104, Jul. 16, 2020. [Online]. Available: https://www.etsi.org/deliver/etsi_ts/138100_138199/138104/16.04.00_60/ts_138104v160400p.pdf
[47] Y. Guangrong, D. Aixian, H. Hao, G. Jianmei, and W. Lei, "Fractionally spaced equalization algorithms in 60GHz communication system," *IEEE China Commun.*, vol. 11, no. 6, pp. 23–31, Jun. 2014.
[48] G. Qiao, S. Gan, S. Liu, and Q. Song, "Self-interference channel estimation algorithm based on maximum-likelihood estimator in in-band full-duplex underwater acoustic communication system," *IEEE Access*, vol. 6, pp. 62324–62334, 2018.
[49] S. Talwar, M. Viberg, and A. Paulraj, "Blind separation of synchronous co-channel digital signals using an antenna array. I. algorithms," *IEEE Trans. Signal Process.*, vol. 44, no. 5, pp. 1184–1197, May 1996.
[50] J. G. McMichael and K. E. Kolodziej, "Optimal tuning of analog self-interference cancellers for full-duplex wireless communication," in *Proc. 50th Annu. Allerton Conf. Commun. Control Comput.*, 2012, pp. 246–251.
[51] G. Shao, "Baseband self-interference cancellation in full-duplex massive-MIMO communication systems," M.Sc. thesis, Dept. Elect. Comput. Eng., McGill Univ., Montreal, QC, Canada, 2023.
[52] M. Mahmood, A. Koc, D. T. Nguyen, R. Morawski, and T. Le-Ngoc, "Sub-array selection in full-duplex massive MIMO for enhanced self-interference suppression," in *Proc. IEEE Glob. Commun. Conf.*, Kuala Lumpur, Malaysia, 2023, pp. 5835–5840 doi: 10.1109/GLOBECOM54140.2023.10436977.

THO LE-NGOC (Life Fellow, IEEE) received the B.Eng. degree in electrical engineering, the M.Eng. degree in microprocessor applications, from McGill University, Montreal, QC, Canada, in 1976 and 1978, respectively, and the Ph.D. degree in digital communications, from the University of Ottawa, ON, Canada, in 1983. From 1977 to 1982, he was with Spar Aerospace Ltd., Montreal, where he involved in the development and design of satellite communications systems. From 1982 to 1985, he was with SR Telecom Inc., Montreal, where he developed the new point-to-multipoint DA-TDMA/TDM Subscriber Radio System SR500. From 1985 to 2000, he was a Professor with the Department of Electrical and Computer Engineering, Concordia University, Montreal. Since 2000, he has been with the Department of Electrical and Computer Engineering, McGill University. His research focuses on broadband digital communications. He is a Distinguished James McGill Professor, and Fellow of the Engineering Institute of Canada, Canadian Academy of Engineering, and Royal Society of Canada. He was the recipient of the 2004 Canadian Award in Telecommunications Research and IEEE Canada Fessenden Award, in 2005.

YUANZHE GONG (Graduate Student Member, IEEE) received the B.Eng. (Hons.) degree in electrical and computer engineering from McGill University, Montreal, Canada, in 2020, where he is currently working toward the Ph.D. degree in electrical engineering. Since 2018, he has been a Teaching Assistant with Electrical and Computer Engineering Department, McGill University. His research interests include, but not limited to wireless communications, antenna design, metamaterial absorbers, massive MIMO, and full-duplex. He was the recipient of McGill Engineering Doctoral Award by McGill University.

MOBEEN MAHMOOD (Graduate Student Member, IEEE) received the B.Sc. (Hons.) degree in electrical engineering from the University of Engineering and Technology, Taxila, Pakistan, in 2013, and the M.Sc. (Hons.) degree in electrical engineering from the American University of Sharjah (AUS), Sharjah, UAE, in 2019. He is currently working toward the Ph.D. in electrical engineering with McGill University, Montreal, QC, Canada. From 2014 to 2017, he was with China Mobile Pakistan, Islamabad, Pakistan. His main research interests include massive MIMO, hybrid beamforming, AI-enable wireless networks, UAV, and full-duplex communications. He was the recipient of AUS teaching assistantship, AUS research assistantship, Fonds de Recherche du QuÃ©bec-Nature and Technologies (FRQNT), IEEE VTS Student Travel Award, IEEE Canada Vehicular Technologies Grant, McGill Graduate Research Enhancement and Travel (GREAT) Award, McGill Graduate Excellence Fellowship, McGill Engineering Class of 1936 Fellowship, and J.W.McConnell Memorial Fellowship as part of McGill Engineering Doctoral Award (MEDA).

ASIL KOC (Graduate Student Member, IEEE) received the B.Sc. (Hons.) degree in electronics and communication engineering, the M.Sc. (Hons.) degree in telecommunication engineering from Istanbul Technical University, Istanbul, Türkiye, in 2015 and 2017, respectively, and the Ph.D. degree in electrical engineering from McGill University, Montreal, Canada, in 2022. From 2015 to 2017, he was a Research and Teaching Assistant with Electronics and Communication Engineering Department, Istanbul Technical University. From 2017 to 2022, he was a Lecturer and Teaching Assistant with Electrical and Computer Engineering Department, McGill University. In 2022, he was a Mitacs Accelerate Intern with Huawei Technologies Canada, Ottawa, ON, Canada. His research interests include AI/ML based wireless communications, massive MIMO, full-duplex, millimeter-wave/terahertz, beamforming, and reconfigurable intelligent surface (RIS). He was the recipient of Erasmus Scholarship by European Union, McGill Engineering Doctoral Award, IEEE ComSoc Student Travel Grant, Graduate Research Enhancement and Travel Award by McGill University, and STARaCom Collaborative Grant by the FRQNT.

ROBERT MORAWSKI received the B.Sc. and M.Sc. degrees in electrical and computer engineering from Concordia University, Montreal, QC, Canada, in 1997 and 2000 respectively. He is currently a Research Engineer and Lab Manager with Broadband Communications Research Lab, ECE Department, McGill University, Montreal. His research focuses on the design and implementation of prototype architectures for next-generation wireless communications

JAMES GARY GRIFFITHS is currently a Senior Principal Researcher with the Canada Research Centre of Huawei Technologies, Ottawa, ON, Canada. He has more than 25 years of experience in the research and development of wireless and wired communication, sensor technologies, specializing in RF subsystems for sensors, hybrid fiber coaxial, and wireless terrestrial and satellite based communications. His research focuses on full duplex wireless communication techniques.

PHILIPPE GUILLEMETTE is currently a Principal Engineer with the Canada Research Centre of Huawei Technologies, Ottawa, ON, Canada. He has more than 20 years of experience in research and development in wireless communication technology, spanning various terrestrial and satellite communication systems. He has wide technical knowledge base covering digital signal processing in wireless physical layer applications as well as radio performances of electronic devices. His research interests include CFR/DPD and self-interference cancellation of mMIMO related full duplex technologies and their wireless applications.

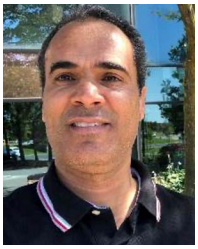

JAMAL ZAID (Member, IEEE) received the B.A.Sc. degree in microwaves engineering from Electrical and Electronic College, Bani Walid, Libya, in 1997, the M.A.Sc. degree in communications and microwave engineering from the Academy of Graduate studies, Tripoli, Libya, in 2008, and the Ph.D. degree in telecommunication from the University of Quebec, Quebec City, QC, Canada, in 2018. From 2008 to 2013, he was an Assistant Professor and the Head of Communications Department, the Higher Institute of Comprehensive Professions, Bani Walid. He is currently a Senior Engineer with the Research and Development Center of Huawei Technologies, Ottawa, ON, Canada. His research interests include antenna design, coupling reduction for multiple-input and multiple-output (MIMO), full duplex system, radio frequency identification (RFID), frequency selective surface (FSS), rlectromagnetic bandgap (EBG), wireless sensor, and antenna miniaturization. Dr. Zaid was the recipient of Innovation Pioneer Award 2020 from the Research and Development Center of Huawei Technologies.

PEIWEI WANG received the B.Eng. degree in computer engineering and the M.Sc. degree in computer science, from Chongqing University, Chongqing, China, in 1982 and 1987, respectively. From 1995 to 1997, he was a Visiting Scholar with the Department of Electrical and Computer science, The University of Texas at Austin, Austin, TX, USA. From 1998 to 2013, he was a CDMA/DSP designer, architect of wireless systems with Nortel Networks and BlackBerry. In 2014, he joined Huawei Canada, where he is currently leading the R&D team for full duplex in wireless applications.